AMERICAN SOCIETY FOR MICROBIOLOGY | Molecular and Cellular Biology®

RESEARCH ARTICLE

Scaffolding Protein IQGAP1 Is Dispensable, but Its Overexpression Promotes Hepatocellular Carcinoma via YAP1 Signaling

Evan R. Delgado,[a] Hanna L. Erickson,[b] Junyan Tao,[a] Satdarshan P. Monga,[a] Andrew W. Duncan,[a] Sayeepriyadarshini Anakk[b,c]

[a]Department of Pathology, McGowan Institute for Regenerative Medicine, Pittsburgh Liver Research Center, University of Pittsburgh, Pittsburgh, Pennsylvania, USA
[b]Department of Molecular and Integrative Physiology, University of Illinois at Urbana-Champaign, Urbana, Illinois, USA
[c]Cancer Center at Illinois, University of Illinois at Urbana-Champaign, Urbana, Illinois, USA

Evan R. Delgado and Hanna L. Erickson are co-first authors. Evan R. Delgado was determined to be the first, as he brought additional mechanistic ideas with YAP and NUAK2 to the manuscript.
Andrew W. Duncan and Sayeepriyadarshini Anakk are co-senior authors.

ABSTRACT IQ motif-containing GTPase-activating protein 1 (IQGAP1) is a ubiquitously expressed scaffolding protein that is overexpressed in a number of cancers, including liver cancer, and is associated with protumorigenic processes, such as cell proliferation, motility, and adhesion. IQGAP1 can integrate multiple signaling pathways and could be an effective antitumor target. Therefore, we examined the role of IQGAP1 in tumor initiation and promotion during liver carcinogenesis. We found that ectopic overexpression of IQGAP1 in the liver is not sufficient to initiate tumorigenesis. Moreover, we report that the tumor burden and cell proliferation in the diethylnitrosamine-induced liver carcinogenesis model in *Iqgap1*$^{-/-}$ mice may be driven by MET signaling. In contrast, IQGAP1 overexpression enhanced YAP activation and subsequent NUAK2 expression to accelerate and promote hepatocellular carcinoma (HCC) in a clinically relevant model expressing activated (S45Y) β-catenin and MET. Here, increasing IQGAP1 expression *in vivo* does not alter β-catenin or MET activation; instead, it promotes YAP activity. Overall, we demonstrate that although IQGAP1 expression is not required for HCC development, the gain of IQGAP1 function promotes the rapid onset and increased liver carcinogenesis. Our results show that an adequate amount of IQGAP1 scaffold is necessary to maintain the quiescent status of the liver.

KEYWORDS IQGAP1, MET, scaffold protein, YAP, liver cancer

Liver cancer has a high mortality rate due to limited effective systemic therapies (1). For hepatocellular carcinoma (HCC), the major form of primary liver cancer, a large portion of cases are diagnosed at advanced stages (2), and only two systemic therapies extend overall survival by a few months (1, 3). Both of these therapies function as multikinase inhibitors, highlighting the role of multiple distinct signaling pathways in promoting tumorigenesis (1, 3). Scaffolding proteins are large multidomain proteins that can simultaneously organize and regulate multiple signaling pathways (4) and would make an effective anticancer target. However, the role of scaffolding proteins in promoting HCC is still largely unknown.

IQ motif-containing GTPase-activating protein 1 (IQGAP1) is a pleiotropic, multidomain scaffolding protein that is overexpressed in many types of human cancer (5), including 60 to 80% of HCCs (6–9), and this overexpression is associated with worse clinical outcomes (8). IQGAP1 interacts with protumorigenic processes, including kinase signaling, cell proliferation, motility, and adhesion (5). Furthermore, *in vivo* studies

Citation Delgado ER, Erickson HL, Tao J, Monga SP, Duncan AW, Anakk S. 2021. Scaffolding protein IQGAP1 is dispensable, but its overexpression promotes hepatocellular carcinoma via YAP1 signaling. Mol Cell Biol 41:e00596-20. https://doi.org/10.1128/MCB.00596-20.

Address correspondence to Andrew W. Duncan, duncana@pitt.edu, or Sayeepriyadarshini Anakk, anakk@illinois.edu.

Received 17 November 2020
Returned for modification 21 December 2020
Accepted 14 January 2021
Accepted manuscript posted online 1 February 2021
Published 24 March 2021

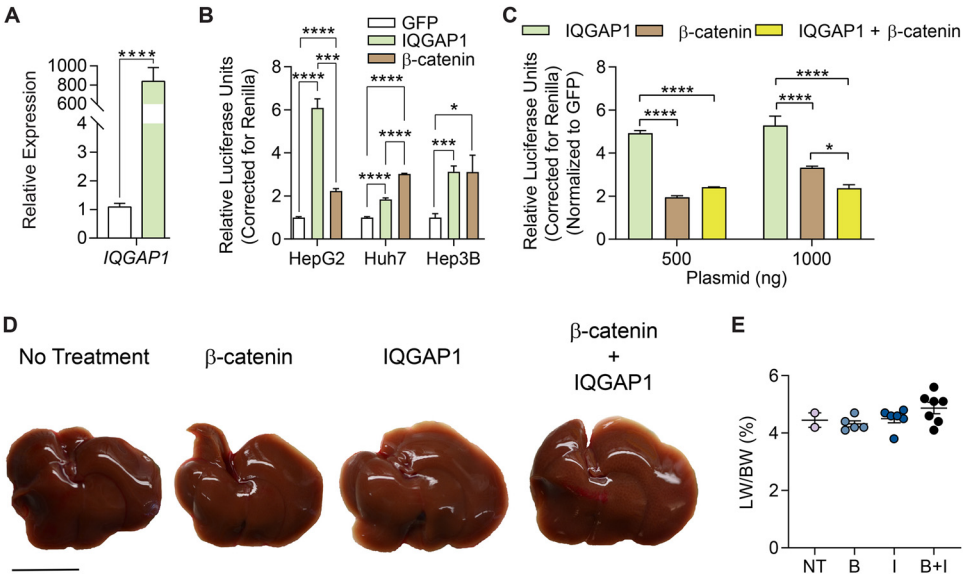

FIG 1 IQGAP1 does not promote β-catenin-driven HCC. (A) HepG2 cells were transfected with GFP or IQGAP1 constructs for 72 h. Expression for *IQGAP1* was normalized to *B2M*. (B) HepG2, Huh7, and Hep3B cell lines were transfected with control, IQGAP1, or (S45Y) β-catenin expression constructs for 72 h. Wnt/β-catenin activity was measured by the TOPFlash luciferase reporter assay and corrected for renilla luciferase. (C) HepG2 cells were transfected with GFP, IQGAP1, or (S45Y) β-catenin expression constructs for 72 h. Additionally, cells were also transfected with IQGAP1 and (S45Y) β-catenin constructs together. Wnt/β-catenin activity was measured and analyzed as previously described. (D) Representative livers from nontreated, (S45Y) β-catenin, IQGAP1, or (S45Y) β-catenin plus IQGAP1 groups. (E) Liver weight to body weight (LW/BW) ratio. Scale bar is 2.5 cm. Graphs show means ± SEM and dots represent individual mice. Student's *t* test was used to determine significance. *, $P < 0.05$; ***, $P < 0.001$; ****, $P < 0.0001$.

demonstrate that increased IQGAP1 expression can promote tumor growth, indicating that IQGAP1 is an effective molecular target for HCC (10–12). However, other studies revealed that deletion of IQGAP1 in cancer cells and/or stromal cells can also enhance tumorigenesis by modulating transforming growth factor (TGF) signaling (13, 14) and adherens junction stability (15).

To understand these contradictory studies, in this paper we carefully investigated the role for IQGAP1 in hepatic tumorigenesis by directly comparing IQGAP1 overexpression and IQGAP1 knockout (*Iqgap1*$^{-/-}$) mouse models of HCC. We show that IQGAP1 overexpression by itself does not cause tumorigenesis, while *Iqgap1* deletion caused a modest increase in HCC incidence and multiplicity in the diethylnitrosamine (DEN) model of liver cancer. Depletion of IQGAP1 in liver cancer cells resulted in elevated levels and activation of the tyrosine kinase receptor MET, which could contribute to increased tumor burden. Importantly, we show that the overexpression of IQGAP1 promotes rapid HCC progression in a transposon-based tumor model induced by β-catenin and MET overexpression, which is mediated by the YAP1-NUAK2 kinase pathway. Thus, the data demonstrate that overexpression of IQGAP1 can promote the development of liver tumors in mice in the background of additional oncogenic signals. Our findings underscore that molecular expression of liver tumors should be considered when developing new therapies for HCC.

RESULTS

IQGAP1 overexpression in mouse liver is insufficient to initiate tumorigenesis. *In vitro* studies have previously shown that IQGAP1 enhances the Wnt/β-catenin pathway (9, 16). To verify this, we overexpressed IQGAP1 in liver cancer cell lines (Fig. 1A) and found a 2- to 6-fold increase in Wnt/β-catenin activity, as measured by the TOPFlash reporter assay, which is consistent with reporter activity induced by human

activated (S45Y) β-catenin that resists proteasomal degradation (Fig. 1B). Coexpression of IQGAP1 and active β-catenin was neither additive nor synergistic (Fig. 1C).

Since IQGAP1 expression is elevated in the majority of HCC cases (6, 7), we tested if IQGAP1 overexpression could promote HCC development *in vivo*. To do this, we overexpressed IQGAP1 with or without human activated (S45Y) β-catenin using the hydrodynamic tail vein injection (HDTVI) with the Sleeping Beauty (SB) transposase (referred to here as the transposon system). Briefly, the transposon system is a nonviral method for long-term expression of plasmids in a subset of hepatocytes (17–20). Five to 40% of hepatocytes are transduced within 24 h, and transposon-mediated target gene integration occurs over 4 days (18, 19). Up to 1% of hepatocytes become stably transduced (18, 19). Seventeen weeks after HDTVI, mice injected with β-catenin alone were tumor free, which is consistent with previous observations (17) (Fig. 1D). Moreover, mice injected with IQGAP1 alone or in combination with β-catenin also failed to develop HCC or any changes to the ratio of liver weight to body weight (LW/BW) (Fig. 1E). Together, our data indicate that IQGAP1-induced β-catenin activity occurs *in vitro*, while IQGAP1 (either alone or combined with activated β-catenin) fails to promote HCC development *in vivo*.

DEN-induced tumorigenesis persists in IQGAP1-deleted livers. We next asked whether IQGAP1 is required for hepatic tumorigenesis. Here, we used the DEN model of liver cancer, a reliable method for chemical hepatic carcinogenesis (20). Following an established published protocol (21), we treated male *Iqgap1*$^{+/+}$, *Iqgap1*$^{+/-}$, and *Iqgap1*$^{-/-}$ mice with 5 mg/kg DEN via intraperitoneal injection at 12 to 15 days of age and assessed tumor burden 20 and 50 weeks posttreatment to characterize both microscopic and macroscopic nodules, respectively. The number of proliferating, Ki-67-positive hepatocytes 24 h after DEN administration was similar for each group, indicating that *Iqgap1* deletion does not affect early-stage damage-induced proliferation (Fig. 2A and B). No macroscopic nodules were observed at 20 weeks, but lesions were observed 50 weeks after DEN treatment (Fig. 2C). Tumor incidence (Fig. 2D) and multiplicity (Fig. 2E) were modestly higher in *Iqgap1*$^{-/-}$ than *Iqgap1*$^{+/-}$ mice. Notably, the liver weight after DEN treatment increased equally between *Iqgap1*$^{+/+}$, *Iqgap1*$^{+/-}$, and *Iqgap1*$^{-/-}$ mice (Fig. 2F). These results suggest that deletion of IQGAP1 does not reduce the liver tumor burden.

We next confirmed that deletion of *Iqgap1* did not result in compensatory expression changes in *Iqgap2* and *Iqgap3*. Of the three isoforms, IQGAP1 has a broad tissue distribution and is more frequently altered in cancer (22). As expected, *Iqgap1* was induced in *Iqgap1*$^{+/+}$ tumors relative to the surrounding healthy liver, and the *Iqgap1*$^{+/-}$ mice exhibited an approximately 50% reduction in *Iqgap1* expression compared to controls (Fig. 2G). *Iqgap2* is more highly expressed in the control liver (*Iqgap1*$^{+/+}$ liver Cq = 18 to 19) than *Iqgap1* (*Iqgap1*$^{+/+}$ liver Cq = 23 to 24) but is decreased in tumor tissue (Fig. 2G). Whereas *Iqgap3* expression is low in the quiescent livers (*Iqgap1*$^{+/+}$ liver Cq = 30 to 31), it is observed in proliferating cells (23, 24) and dramatically induced in tumor tissue (Fig. 2G). Notably, the expression pattern of neither *Iqgap2* nor *Iqgap3* was altered by *Iqgap1* deletion. Thus, the effect of IQGAP1 deletion on tumor burden occurs independently of *Iqgap2* and *Iqgap3* dysregulation.

IQGAP1 loss does not cause differential molecular dysregulation in HCC. We next asked if there were any fundamental differences in the molecular characteristics of *Iqgap1*$^{+/+}$, *Iqgap1*$^{+/-}$, and *Iqgap1*$^{-/-}$ tumors. First, liver cancer can be divided into at least six molecular subtypes (G1 to G6) depending on their gene expression patterns (Fig. 3A) (25). We analyzed markers of proliferation, lipogenesis, inflammation, gluconeogenesis, and angiogenesis (Fig. 3A) that have been previously identified to correspond to these distinct molecular subtypes of human HCC (25, 26). No differences in gene expression patterns were observed between groups, and based on expression changes of 5 of 7 genes (*Rrm2*, *Tgfbr1*, *Fasn*, *Pepck*, and *Angpt2*), tumors aligned with the G3 subtype regardless of IQGAP1 expression. Second, since DEN-induced tumors are frequently driven by mutations in *Hras* (27, 28), we performed targeted DNA sequencing to examine the mutation spectrum among the groups. Despite varied tumor burden between *Iqgap1*$^{+/+}$, *Iqgap1*$^{+/-}$, and *Iqgap1*$^{-/-}$ tumors, DEN-induced

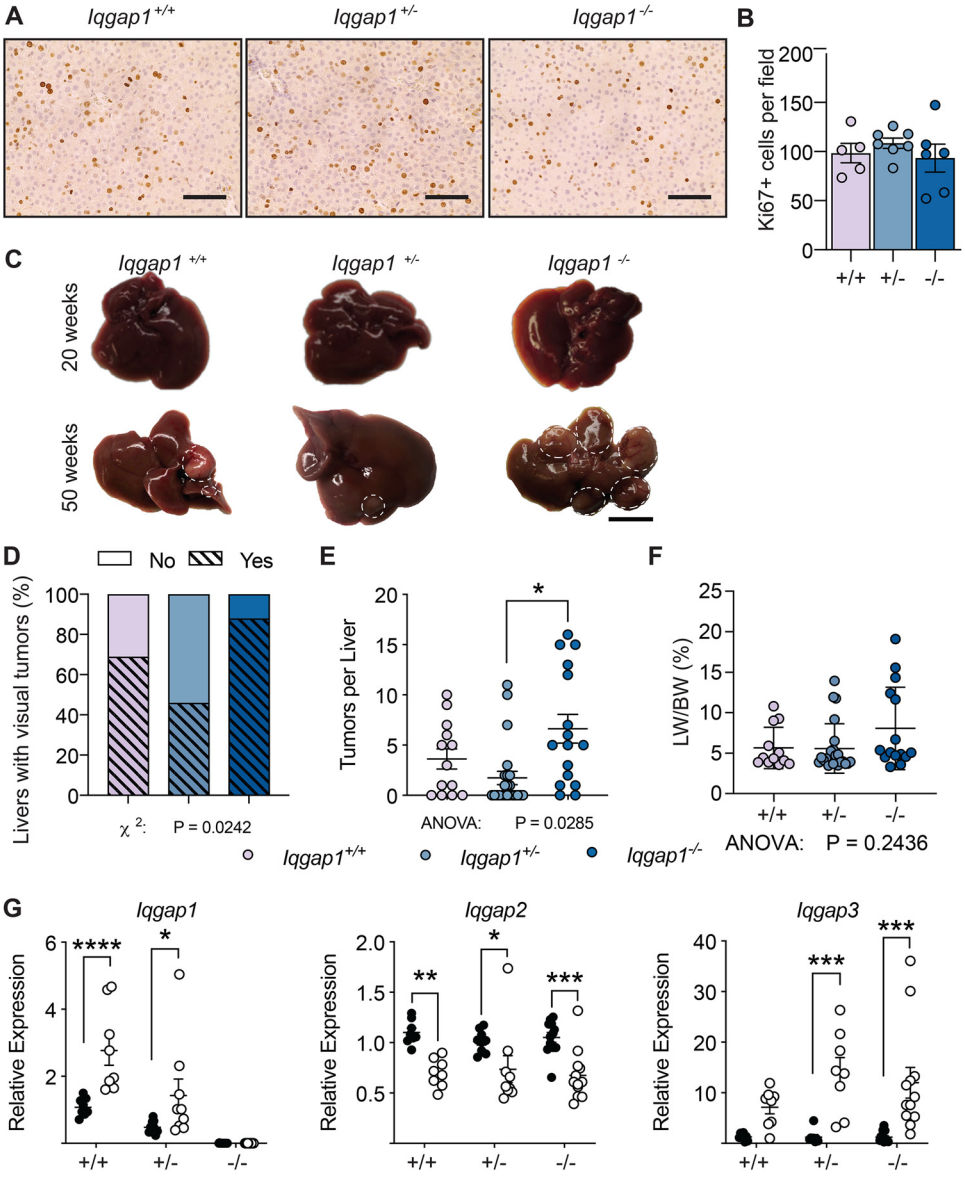

FIG 2 IQGAP1 deletion does not inhibit liver tumor development. Male *Iqgap1*$^{+/+}$ ($n = 13$), *Iqgap1*$^{+/-}$ ($n = 24$), and *Iqgap1*$^{-/-}$ ($n = 16$) mice were treated intraperitoneally with 5 mg/kg diethylnitrosamine (DEN) in sterile PBS at 12 to 15 days of age. At 1 year, tumor burden was assessed. (A) Representative Ki-67 immunohistochemistry images of livers of P15 mice 24 h after DEN injection. Scale bar is 50 μm. (B) Quantification of Ki-67-positive cells per field ($n = 5$ *Iqgap1*$^{+/+}$, 7 *Iqgap1*$^{+/-}$, and 6 *Iqgap1*$^{-/-}$ mice). (C) Representative photos of gross livers at one year. Tumor nodules are indicated by a dashed border. Scale bar is 1 cm. (D) Tumor incidence based on presence of visible liver nodules. (E) Tumor multiplicity was measured by counting the number of visible tumors per liver. (F) Liver weight normalized to body weight divided into low and high groups. (G) Gene expression of *Iqgap1*, *Iqgap2*, and *Iqgap3* in tumor-adjacent liver tissue and tumor tissue normalized to *Gapdh* expression. Values are displayed as means ± SEM. For tumor incidence, χ^2 test was used to determine significance between all 3 groups. For tumor multiplicity and largest tumor size, one-way ANOVA with Bonferroni's multiple-comparison test was used to determine significance between groups. For liver-to-body-weight ratio, two-way ANOVA with Bonferroni's multiple-comparison test was used to determine significance between groups. For gene expression, two-way ANOVA with Tukey's multiple-comparison test was used to determine significance. *, $P < 0.05$; **, $P < 0.01$; ***, $P < 0.001$; ****, $P < 0.0001$.

mutations in *Braf*, *Egfr*, and *Hras* were conserved among them (Fig. 3B to E). Finally, IQGAP1 has been shown to promote epithelial-mesenchymal transition (EMT) (29). Therefore, we examined the protein levels of markers of this process, including MMP2, E-cadherin, N-cadherin, and CDC42, and found no significant difference between the groups (Fig. 3F). Taken together, the data indicate that DNA alterations, tumor subtypes, and EMT are unaffected by IQGAP1 loss in the DEN tumor model.

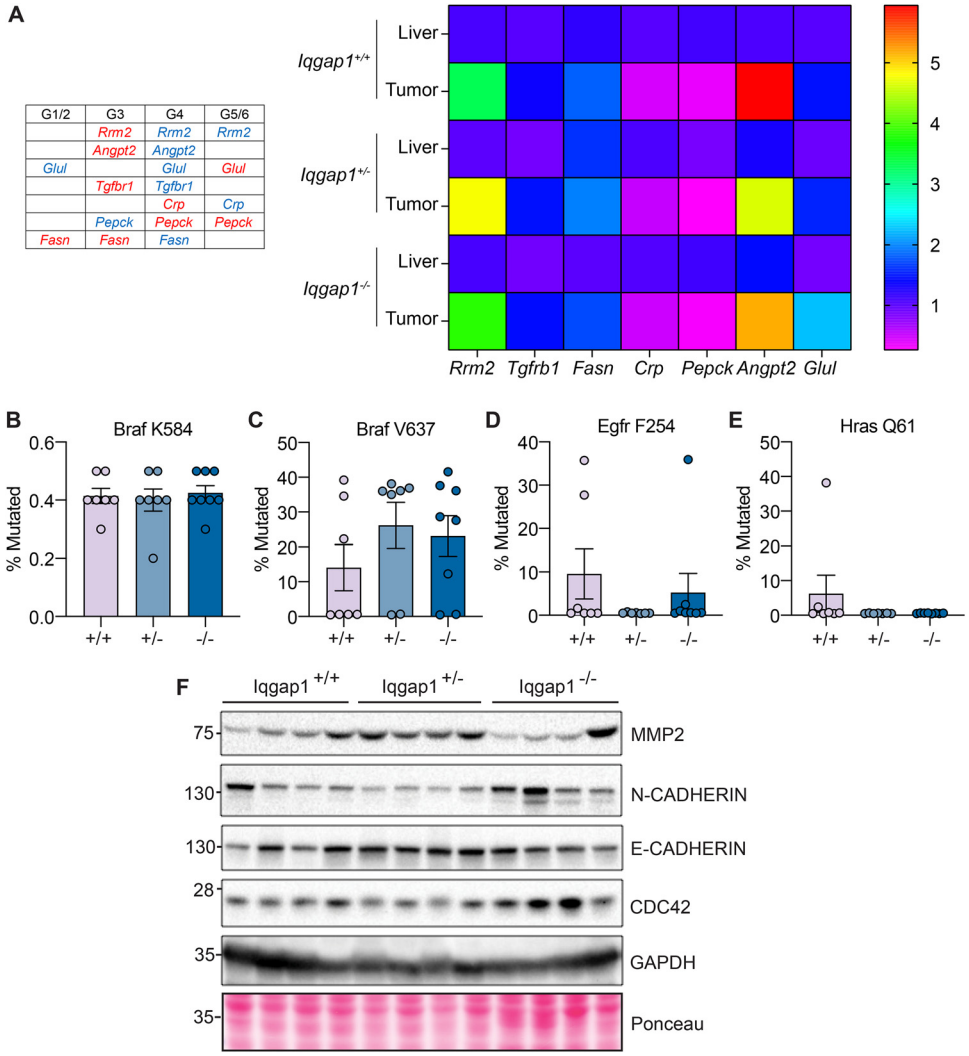

FIG 3 Hepatic gene expression, DEN-induced mutations, and epithelial-mesenchymal transition (EMT) are unaffected by *Iqgap1* loss. (A) The table shows gene expression patterns correlating with molecular subtypes of HCC adapted from Boyault et al. (25). Red represents upregulated genes. Blue represents downregulated genes. Gene expression of *Rrm2*, *Tgfbr1*, *Fasn*, *Crp*, *Pepck*, *Angpt2*, and *Glul* in tumor-adjacent liver tissue and tumor tissue normalized to *Gapdh* expression. (B to E) DNA mutation frequency at select codons in tumors of mice 50 weeks after DEN injection ($n = 7$ *Iqgap1*$^{+/+}$, 7 *Iqgap1*$^{+/-}$, and 8 *Iqgap1*$^{-/-}$ mice). (F) Immunoblot of EMT markers MMP2, N-cadherin, E-cadherin, and Cdc42 in tumors of *Iqgap1*$^{+/+}$, *Iqgap1*$^{+/-}$, and *Iqgap1*$^{-/-}$ mice 50 weeks after DEN treatment ($n = 4$ mice per group). For gene expression, two-way ANOVA with Tukey's multiple-comparison test was used to determine significance. One-way ANOVA with Bonferroni multiple-comparison test was used to compare groups in panels B to E. *, $P < 0.05$; **, $P < 0.01$; ***, $P < 0.001$; ****, $P < 0.0001$.

Dysregulated MET signaling contributes to increased cell proliferation in *Iqgap1*$^{-/-}$ tumors. Since the incidence and tumor multiplicity were modestly higher in *Iqgap1*$^{-/-}$ mice, we investigated if the proliferation of the tumors differed between the genotypes. Ki-67 staining, a marker of nonquiescent cells, revealed increased numbers of Ki-67^{+} cells in tumor tissue compared to healthy adjacent liver, regardless of genotype (Fig. 4A). Within tumor tissue, there were nearly twice as many Ki-67^{+} cells in *Iqgap1*$^{-/-}$ compared to WT mice. To determine why *Iqgap1*$^{-/-}$ tumors have more proliferating cells, we investigated several oncogenic pathways implicated in hepatocellular carcinogenesis. Because IQGAP1 can regulate RAF-MEK-ERK signaling (10, 30–32), we checked tumors for phosphorylated ERK (P-ERK) and found positive staining in 17/23 *Iqgap1*$^{+/+}$ (74%), 17/18 *Iqgap1*$^{+/-}$ (94%), and 18/28 *Iqgap1*$^{-/-}$ (64%) tumors (Fig. 4B), indicating ERK signaling is active across all groups. We next analyzed Wnt/β-catenin signaling by

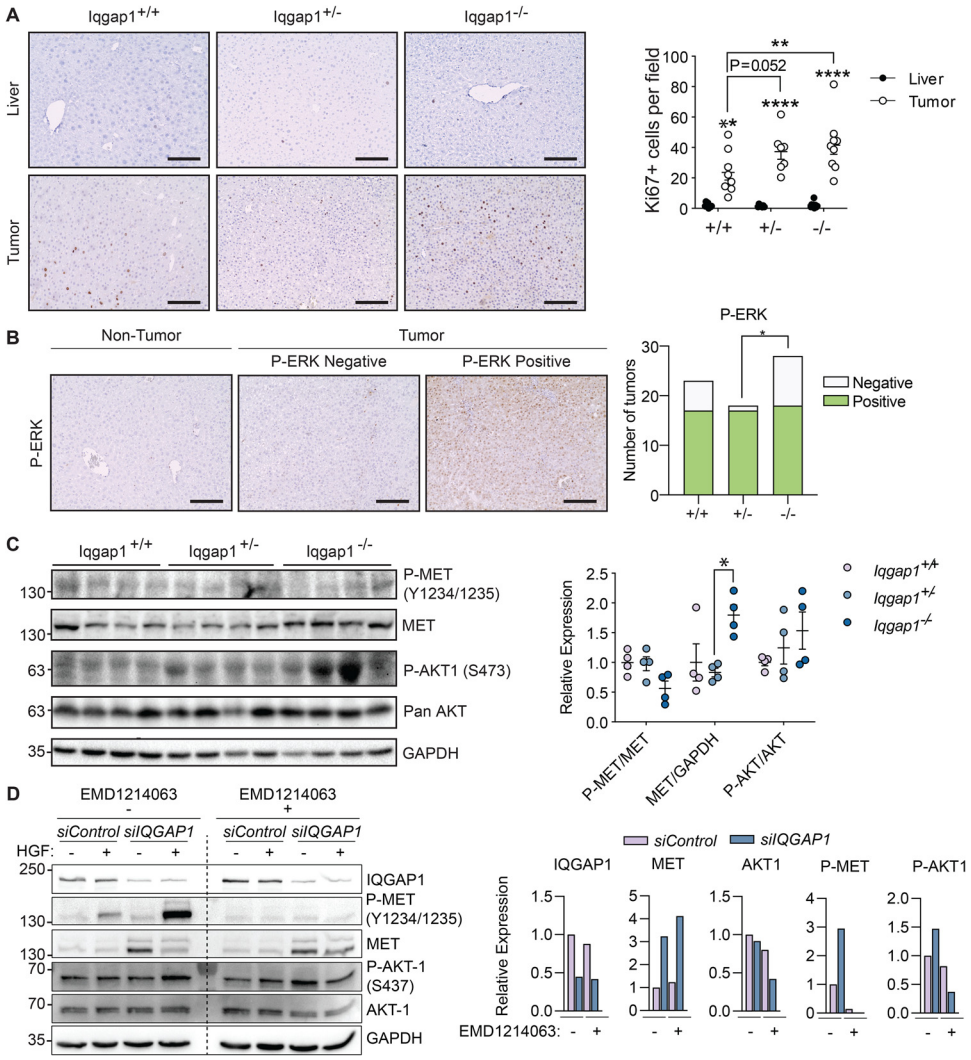

FIG 4 IQGAP1 knockdown enhances MET expression. (A) Representative images of anti-Ki-67 immunohistochemistry staining in liver and tumor tissue of *Iqgap1*$^{+/+}$, *Iqgap1*$^{+/-}$, and *Iqgap1*$^{-/-}$ animals ($n = 9$, 8, and 12 mice per group, respectively). Scale bar is 100 μm. (B) Representative immunohistochemistry images of anti-P-ERK staining in normal liver tissue and tumor tissue classified as either P-ERK negative or P-ERK positive. Scale bar is 100 μm. The number of tumors with each molecular classification ($n = 23$, 18, and 28 *Iqgap1*$^{+/+}$, *Iqgap1*$^{+/-}$, and *Iqgap1*$^{-/-}$ tumors, respectively). (C) Immunoblot of DEN-treated *Iqgap1*$^{+/+}$, *Iqgap1*$^{+/-}$, and *Iqgap1*$^{-/-}$ tumor extracts. Each lane contains extracts from a single mouse and quantified by densitometry. (D) Snu-449 HCC cells were transfected with either Control or *IQGAP1* siRNA for 72 h. Cells were then serum starved overnight and treated with or without HGF (50 ng/μl) and with or without EMD1214063 (10 nM) for 4 h prior to harvest. Whole-cell lysates were immunoblotted for phosphorylated and total forms of specific targets and normalized to GAPDH. Conditions are representative of 3 independent experiments pooled. Quantification of immunoblots with respect to only HGF^{+} conditions by densitometry. Values are displayed as means ± SEM. For ERK staining, two-way paired ANOVA with Tukey's multiple-comparison test was used to assess differences between groups. One-way paired ANOVA with Tukey's multiple-comparison test was used for all others. *, $P < 0.05$.

analyzing the mRNA expression of β-catenin and target genes and found no evidence of differential activation of the Wnt pathway between groups (data not shown). Finally, we investigated the tyrosine kinase receptor MET, which is commonly activated in HCC and has been recently shown to impact IQGAP1 activity (33–37). We measured MET expression and activation in DEN-induced tumors, marked by the phosphorylation of tyrosine residues 1234/1235 of MET (Y1234/1235) (36). Although Y1234/1235 phospho-MET (P-MET) levels remained unchanged between the groups, total MET expression was elevated in *Iqgap1*$^{-/-}$ livers after DEN treatment (Fig. 4C). Phosphorylated AKT-1

(P-AKT-1) S473, a target downstream of MET signaling, however, remained unaltered in *Iqgap1*$^{-/-}$ tissues (Fig. 4C).

We next decided to clarify these data by examining the MET pathway in liver cancer cell lines. Knockdown of IQGAP1 using short interfering RNA (siRNA) increased MET expression 2-fold (Fig. 4D). Further, upon hepatocyte growth factor (HGF) stimulation, IQGAP1 knockdown cells showed increased phosphorylation of MET and AKT-1, suggesting that the loss of *IQGAP1* renders cells highly sensitive to MET pathway activation (Fig. 4D). In addition, treatment of cells with the MET small-molecule inhibitor EMD1214063 blocked MET and AKT-1 phosphorylation after *IQGAP1* loss and HGF stimulation (Fig. 4D). Taken together, these data indicate IQGAP1 depletion increases MET expression and activity, which could facilitate HCC development.

IQGAP1 overexpression exacerbates HCC carcinogenesis in the β-catenin/MET model. Since IQGAP1 overexpression on its own is incapable of initiating HCC development and *Iqgap1* loss only modestly increased HCC burden, we asked if IQGAP1 can exacerbate HCC growth. Here, we used the transposon system to force expression of (S45Y) β-catenin plus MET (B+M) (17). The combination of enhanced Wnt signaling and MET expression promotes downstream signaling events that result in HCC (17). Simultaneous expression of B+M induces microscopic lesions visible by 2 weeks and macroscopic HCC within 6 to 9 weeks, which are 69% genetically similar to human HCC (17).

Using the transposon system, we overexpressed epitope-tagged B+M with or without simultaneous expression of epitope-tagged human IQGAP1 (B+M+I) in WT mice and harvested livers after 4 or 8.5 weeks (Fig. 5A). As early as 4 weeks, tagged β-catenin and MET were expressed in liver lysates in B+M and B+M+I groups compared to nontreated (NT) controls, and tagged IQGAP1 was expressed only in the B+M+I group (Fig. 5B). We also checked expression of *Iqgap* family members and found that *Iqgap2* was unchanged, while *Iqgap3* was elevated in both B+M and B+M+I livers compared to NT controls (Fig. 5C). Upregulation of *Iqgap3* in tumor tissues was also seen in DEN-induced tumors (Fig. 2G), again suggesting that *Iqgap3* induction marks cell proliferation.

Macroscopic disease was not evident after 4 weeks, but at 8.5 weeks, there were visible tumor nodules in both the B+M and B+M+I groups (Fig. 5D). The LW/BW ratio (Fig. 5E) was equivalent after 4 weeks and was 2-fold higher in the B+M+I group at 8.5 weeks compared to those of the controls. Alpha-fetoprotein, a marker of highly aggressive HCC (38–40), was highest in the B+M+I group at 8.5 weeks (Fig. 5F). Microscopic tumor nodules were present at each time point (Fig. 5G). Tumors in B+M and B+M+I groups showed typical HCC morphology, visible by hematoxylin and eosin (H&E) staining, and, as expected for tumors induced by activated β-catenin, HCC nodules were enriched for glutamine synthetase (GS) expression in both groups and at all time points (Fig. 5G). In addition, we measured the expression of genes that differentiate between G1 to G6 molecular subtypes, as described for Fig. 3A, and found changes in 4/7 genes (*Glul*, *Tgfbr1*, *Fasn*, and *Crp*) in B+M and B+M+I tissues, indicating G5/G6 subtypes (Fig. 5H). HCC tumors with activating *CTNNB1* mutations typically fall within the G5/G6 molecular subtypes, which are characterized by low cell proliferation, chromosomal stability, and a lack of inflammatory infiltrates (25, 26). Notably, HCC nodules at 8.5 weeks were advanced and highly necrotic (Fig. 5G). Thus, IQGAP1 overexpression in the B+M tumor model accelerates HCC tumor expansion.

Overexpression of IQGAP1 does not promote HCC formation via enhanced Wnt/β-catenin or MET signaling. Our earlier results indicate that IQGAP1 does not cooperate with β-catenin *in vivo* to promote HCC (Fig. 1D and E), so we asked if this was still the case in the background of B+M. IQGAP1 has been shown to aid β-catenin translocation to the nucleus *in vitro* (9); therefore, we investigated *in vivo* subcellular localization of β-catenin after IQGAP1 overexpression. Cytoplasmic and nuclear fractions from whole liver samples of B+M or B+M+I mice were analyzed. As expected, IQGAP1 cytosolic and nuclear levels were elevated in B+M+I livers compared to B+M (Fig. 6A). Strikingly, B+M+I livers displayed a 3-fold increase in cytosolic β-catenin compared to a modest 1.5-fold increase in the nucleus (Fig. 6A). This result suggests

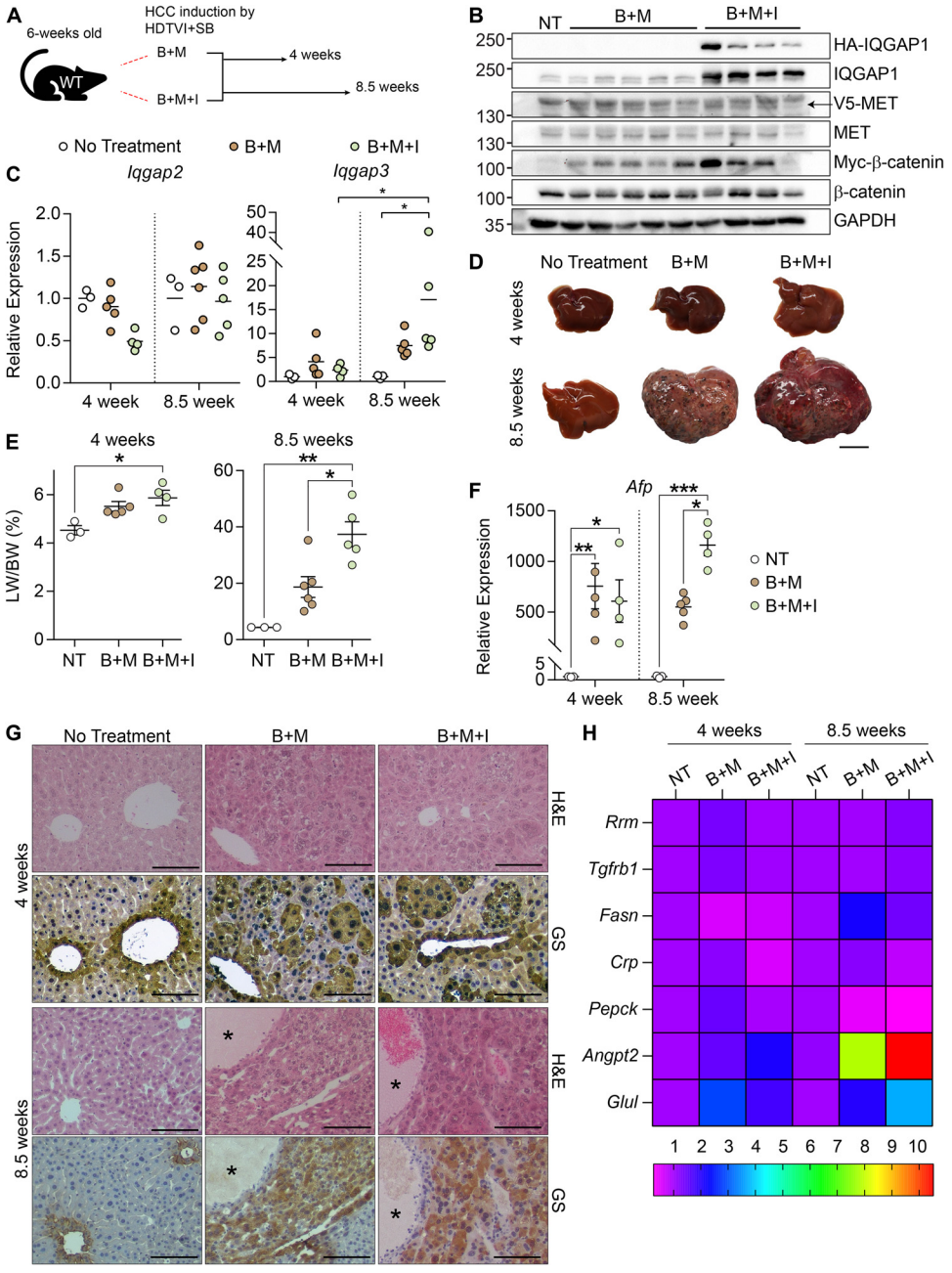

FIG 5 IQGAP1 overexpression increases HCC development in B+M transposon system. (A) Experimental design for Sleeping Beauty transposase groups injected with either B+M or B+M+I and harvested after 4 or 8.5 weeks. (B) Whole liver protein lysates isolated after 4 weeks and analyzed by Western blotting to detect epitope-tagged (HA, V5, or Myc) and total IQGAP1, MET, and β-catenin, normalized to GAPDH. (C) Gene expression of *Iqgap2* and *Iqgap3* in whole livers from 4- and 8.5-week samples from the transposon model. Gene expression was normalized to *Gapdh*. (D) Representative livers from nontreated, B+M, and B+M+I groups. Macroscopic disease is visible as black or white lesions. (E) Liver weight to body weight (LW/BW) ratio. (F) *Afp* expression corrected for *Gapdh*. (G) Serial liver sections from 4-week and 8.5-week mice stained with H&E and GS (brown) to identify β-catenin driven HCCs. Necrotic regions are marked by asterisks. (H) Gene expression for *Rrm2*, *Tgfbr1*, *Fasn*, *Crp*, *Pepck*, *Angpt2*, and *Glul* in whole livers from 4- and 8.5-week samples from the transposon model. Gene expression was normalized to *Gapdh*. Graphs show means ± SEM, and dots represent individual mice. Two-way paired ANOVA with Tukey's multiple-comparison test was used to determine significance between groups in panel E, and Student's t test was used for panel D. *, $P < 0.05$; **, $P < 0.01$; ***, $P < 0.001$. Gross morphology scale bar (C) is 2.5 cm, and histology scale bars (F) are 100 μm.

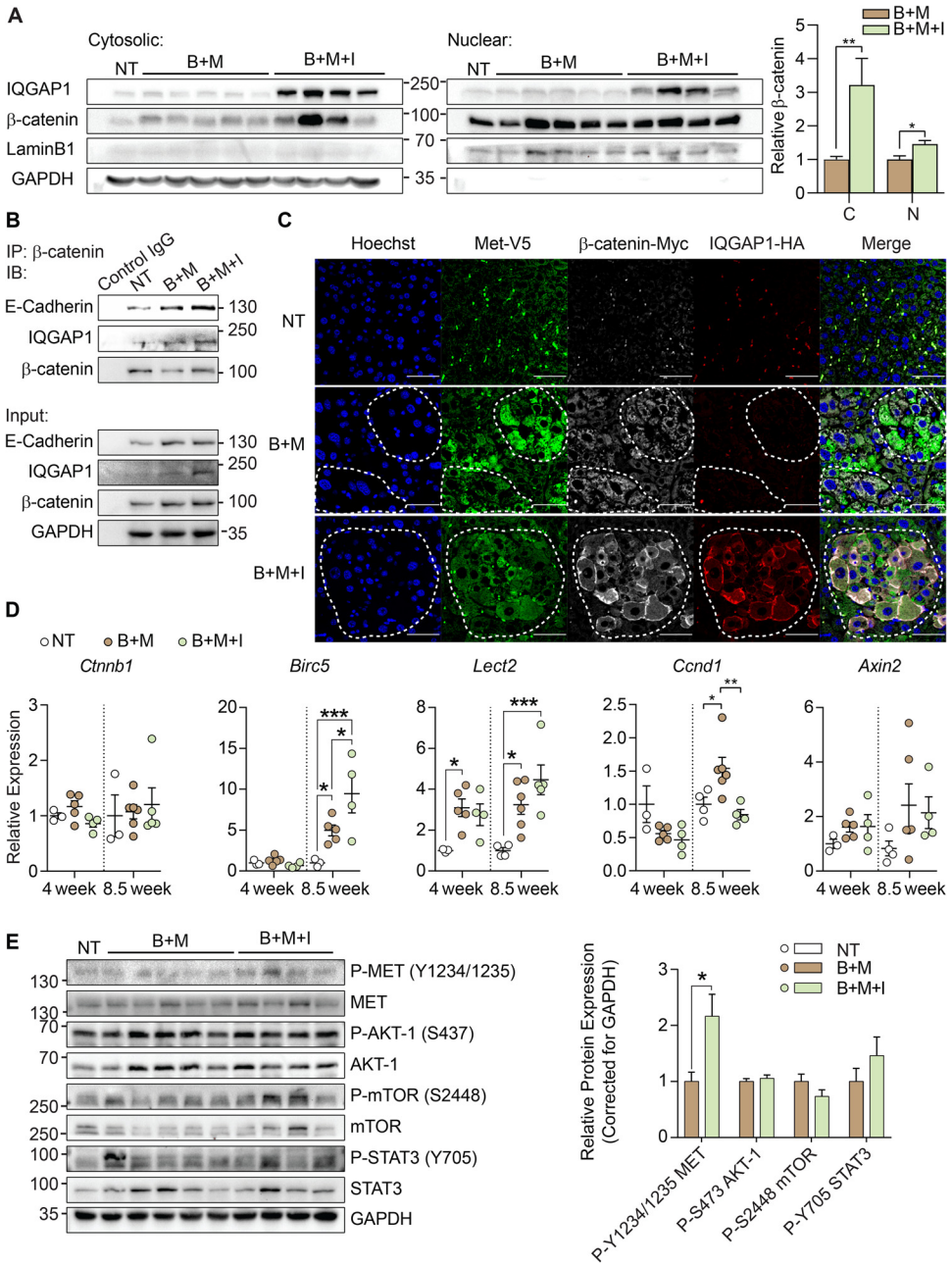

FIG 6 IQGAP1 overexpression does not induce Wnt/β-catenin or MET signaling *in vivo*. (A) Cytosolic and nuclear proteins from whole livers (4-week NT, B+M, and B+M+I) were analyzed for IQGAP1 and β-catenin. Cytosolic protein was normalized to GAPDH and nuclear protein normalized to LaminB1. GAPDH and LaminB1 show purity of cytosolic or nuclear fractions, respectively. (B) Whole liver lysates from NT ($n = 3$), B+M ($n = 5$), or B+M+I ($n = 4$) were pooled and immunoprecipitated (IP) for β-catenin and then immunoblotted (IB) for E-cadherin, IQGAP1, or β-catenin. Sample inputs were probed for E-cadherin, β-catenin, or GAPDH to demonstrate equal amounts of protein from each group and were used for IPs. (C) Liver sections from mice under the HDTVI model for 4 weeks stained for V5 (green), HA (red), or myc (white) to identify nodules by immunofluorescence expressing MET, IQGAP1, and β-catenin, respectively. Tumors under the B+M condition are demarcated by a dashed line. Scale bar is 50 μm. Graphs show means ± SEM, and dots represent individual mice. (D) Expression of *Ctnnb1* and Wnt/β-catenin target genes *Birc5*, *Lect2*, *Ccnd1*, and *Axin2* in whole livers from 4- and 8.5-week samples, normalized to *Gapdh*. (E) Whole-liver protein lysates analyzed by immunoblotting for total and phosphorylated tyrosine residues of MET (Y1234/1235), AKT-1 (S437), mTOR (S2448), and STAT3 (Y705). Phosphorylated protein is normalized to GAPDH and corrected for total respective protein; values are expressed relative to the NT control (set to 1). For panel D, two-way paired ANOVA with Tukey's multiple-comparison test and all others compared via Student's *t* test to determine significance. Graphs show means ± SEM. *, $P < 0.05$; **, $P < 0.01$; ***, $P < 0.001$.

that even though IQGAP1 overexpression leads to a slight enhancement in nuclear β-catenin in the B+M model, the majority of activated β-catenin remains in the cytosol *in vivo*.

Since β-catenin is enriched in the cytosolic fraction of B+M+I samples, we asked if IQGAP1 overexpression enhances the physical interaction between β-catenin and E-cadherin at the cell membrane. Using whole-liver lysates from B+M or B+M+I mice, we coimmunoprecipitated β-catenin and found elevated E-cadherin in B+M+I, indicating that IQGAP1 overexpression enhances β-catenin–E-cadherin interactions (Fig. 6B). Similarly, we found that β-catenin and IQGAP1 colocalize at the cell membrane in B+M+I tissues compared to B+M tissues, where β-catenin was mostly cytoplasmic (Fig. 6C). These data demonstrate that IQGAP1 overexpression increases cytoplasmic and membrane-bound β-catenin expression *in vivo*.

The 1.5-fold increase of nuclear β-catenin in B+M+I samples suggests that Wnt/β-catenin activity is increased; therefore, we directly investigated β-catenin activity in B+M and B+M+I tissues. β-catenin mRNA expression was equivalent in B+M and B+M+I groups (Fig. 6D). After 4 weeks of IQGAP1 coexpression, there were no significant differences in transcript levels of canonical Wnt/β-catenin targets *Birc5*, *Lect2*, *Ccdn1*, *Axin2*, or *Glul* between B+M and B+M+I groups (Fig. 5H and 6D). However, after 8.5 weeks, *Ccdn1* was induced only under the B+M condition, and *Birc5* was elevated in the B+M+I group (Fig. 6H). Since *Birc5* expression is not exclusively controlled by Wnt/β-catenin signaling but can be regulated by the Hippo pathway, our results suggest that IQGAP1 does not enhance β-catenin signaling in the B+M model.

We next examined the MET pathway, since MET is overexpressed in the B+M model and IQGAP1 overexpression is associated with increased MET activity (37). MET is known to activate protumorigenic pathways, including MEK/ERK, phosphatidylinositol 3-kinase (PI3K)/AKT/mTOR, and others, resulting in increased protein phosphorylation (36). We assessed P-MET Y1234/1235 as well as total MET expression in B+M and B+M+I livers (Fig. 6E). Despite 2-fold higher phosphorylated MET at Y1234/1235 in B+M+I, total MET expression as well as the downstream targets of MET activation (AKT-1, mTOR, and STAT3) were comparable (Fig. 6E). These results suggest that the IQGAP1-mediated tumorigenesis is independent of MET pathway activation in the B+M model.

IQGAP1 overexpression drives HCC via Hippo/YAP signaling. We next turned to the Hippo pathway, which can regulate *Birc5* and *Glul* (Fig. 5H and 6D) (41, 42), both of which were dysregulated in the B+M+I livers. Activation of Hippo kinases results in cytoplasmic retention of Yes-associated protein 1 (YAP1), and IQGAP1 has been shown by others to regulate YAP1 level and activity *in vitro* (43, 44). We first investigated YAP activation using a YAP luciferase reporter assay. Liver cancer cells were transfected with IQGAP1 or activated (S127A) YAP1 (Fig. 7A). Overexpression of IQGAP1 alone failed to increase reporter activity compared to green fluorescent protein (GFP). However, coexpression of IQGAP1 with activated YAP1 consistently increased activity 2- to 4-fold compared to cells transfected with activated YAP1 alone (Fig. 7B).

Elevated YAP1 activity is known as an early oncogenic event in HCC (45). To better understand the IQGAP1-YAP1 relationship, we harvested B+M and B+M+I livers after 2 weeks in the transposon system. GS-positive cells were detected in pericentral regions, as expected, but there were 2.5-fold more ectopic GS-positive cell clusters that were 1.5-fold larger in B+M+I samples (Fig. 7C), and 35% of nuclei were positive for nuclear YAP1 in the B+M+I group compared to less than 1% in B+M samples (Fig. 7D). Next, to further verify that IQGAP1 overexpression in the B+M model affects YAP1 signaling *in vivo*, we investigated YAP1 subcellular localization, focusing on the 4-week time point where tumor tissue is abundant but not necrotic (Fig. 5G). YAP1 was lowly detected in the cytoplasm but was elevated 2.5-fold in the B+M+I nuclear fraction compared to B+M (Fig. 7E). Despite increased nuclear YAP1 protein, mRNA expression of *Yap1* and its target genes (*Amotl2*, *Ccn1*, *Ccn2*, and *Jag1*) remained unchanged between B+M and B+M+I groups except for *Ccn2* (Fig. 7F). These data are consistent

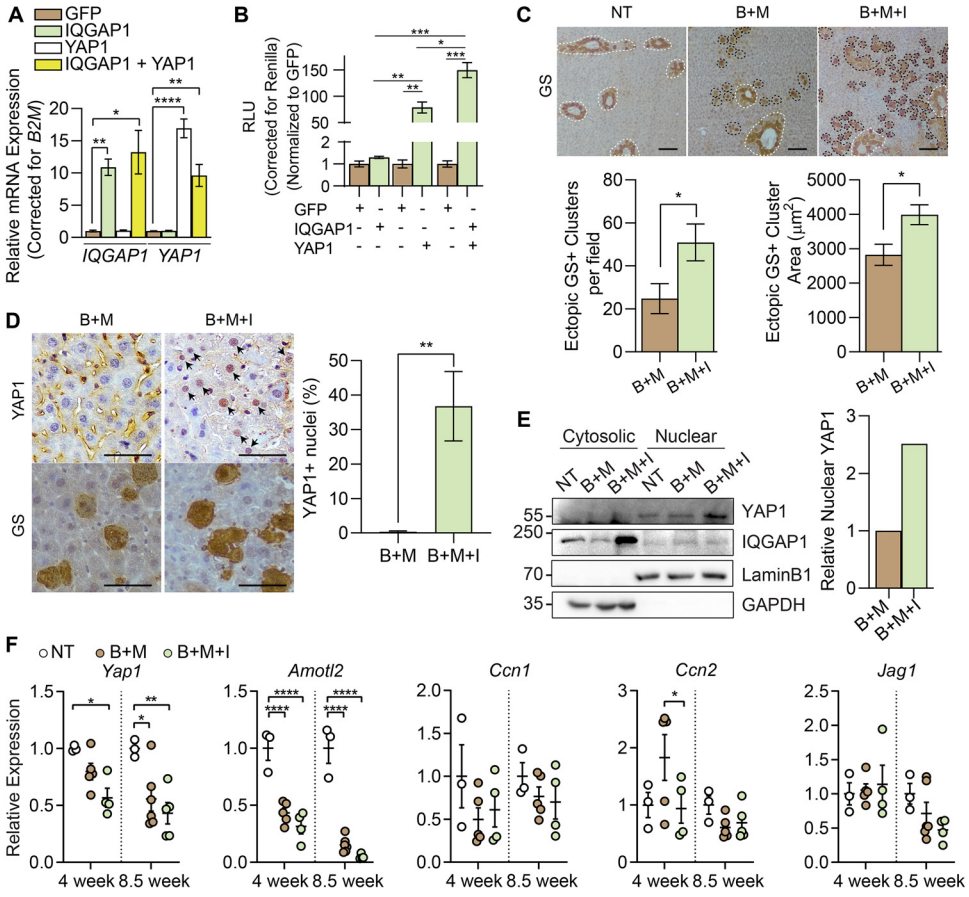

FIG 7 IQGAP1 overexpression drives YAP1 nuclear translocation and activity. (A) HepG2 cells were transfected with 6 μg GFP, 4 μg IQGAP1, or 2 μg (S127A) YAP1 constructs for 24 h. Expression for *IQGAP1* or *YAP1* was normalized to *B2M*. (B) HepG2 cells were transfected with 500, 1,000, or 1,500 ng GFP, 1,000 ng IQGAP1, or 500 ng (S127A) YAP1 expression constructs for 24 h. YAP1 activity was measured using the YAP1 luciferase reporter and corrected using renilla luciferase. (C) Liver sections from 2-week NT, B+M, or B+M+I mice stained with GS (brown) to identify normal pericentral (demarcated by white dashed line) or ectopic (demarcated by black dashed line) regions. Scale bar is 100 μm. (D) Serial liver sections from 2-week mice stained to mark YAP1 nuclei (top, defined by arrows) or GS (bottom). Scale bar is 50 μm. (E) Cytosolic and nuclear protein from whole livers (4-week pooled NT [$n = 3$], B+M [$n = 5$], and B+M+I [$n = 4$]) were analyzed for YAP1 or IQGAP1. Cytosolic protein was normalized to GAPDH and nuclear protein to LaminB1. GAPDH and LaminB1 show purity of cytosolic or nuclear fractions, respectively. (F) Expression of *Yap1* and Hippo/YAP target genes *Amotl2*, *Ccn1*, *Ccn2*, and *Jag1* in whole livers from 4- and 8.5-week samples, normalized to *Gapdh*. Graphs show means ± SEM, and dots represent individual mice. Data in panels A and B are representative of studies replicated in Snu-449 and Huh7 HCC cells. For panel F, two-way paired ANOVA with Tukey's multiple-comparison test was used, and all others were compared using Student's *t* test. *, $P < 0.05$; **, $P < 0.01$; ***, $P < 0.001$; ****, $P < 0.0001$.

with recent findings that reveal *Amotl2*, *Ccn1*, *Ccn2*, and *Jag1* have minimal functional roles in HCC pathogenesis *in vivo* (46–51), even though they are important in tracking hepatoblastoma progression (52–55).

Recently, YAP1-driven HCC tumorigenesis was shown to be mediated by NUAK2 kinase, which positively regulates YAP1 activity in a feed-forward manner (56, 57). We first tested if NUAK2 expression is altered in HCC cells when IQGAP1 and YAP1 are overexpressed. We found that both *NUAK2* mRNA and protein expression are significantly elevated if IQGAP1 and YAP1 are overexpressed together (Fig. 8A and B). Additionally, IQGAP1 and YAP1 cooverexpression contributes to exacerbated cell proliferation (Fig. 8C). While investigating *in vivo* expression of *Nuak2*, we found higher *Nuak2* expression when IQGAP1 is overexpressed in the B+M model at the 4-week time point compared to B+M alone where *Nuak2* is derepressed (Fig. 8D). This is not observed at the 8.5-week time point (Fig. 8D), suggesting that the IQGAP1-YAP1 regulation is lost in late stages of tumorigenesis. Similarly, there is 1.5-fold more NUAK2

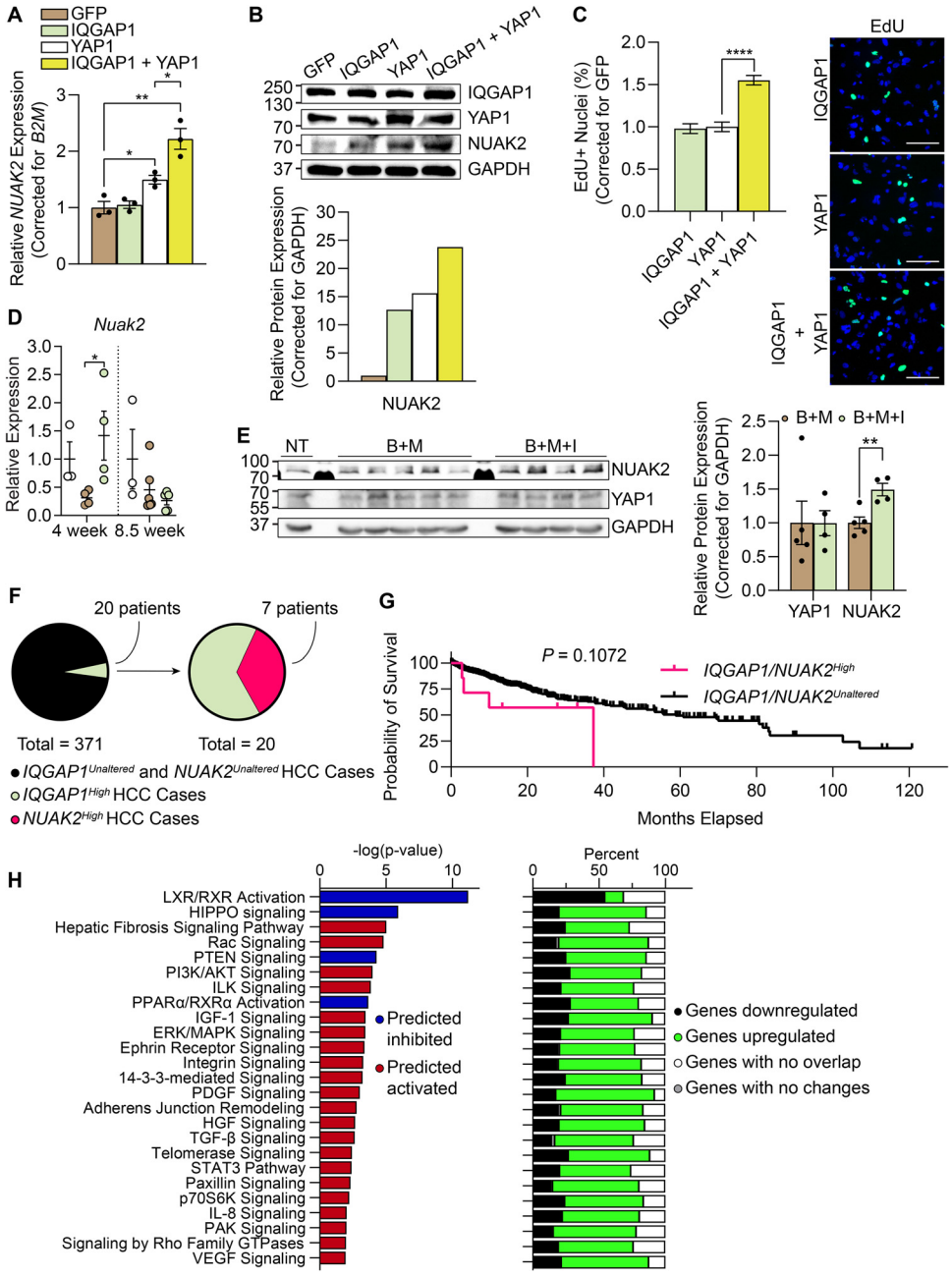

FIG 8 NUAK2 expression is elevated in HCCs with IQGAP1 overexpression. (A) HepG2 cells were transfected with 6 μg GFP, 4 μg IQGAP1, or 2 μg (S127A) YAP1 constructs for 24 h. Expression for *NUAK2* was normalized to *B2M*. (B) Whole-cell lysates were immunoblotted for IQGAP1, YAP1, and NUAK2 and normalized to GAPDH. Conditions presented are representative of 3 independent experiments pooled. (C) Huh7 HCC cells were transfected with 6 μg GFP, 4 μg IQGAP1, or 2 μg (S127A) YAP1 constructs for 24 h. Cells were pulsed with EdU for 30 min prior to fixation and staining for EdU (green) and Hoechst (blue). (D) Expression of *Nuak2* in whole livers from 4- and 8.5-week NT, B+M, and B+M+I samples, normalized to *Gapdh*. (E) Whole-liver protein lysates from 4-week NT, B+M, and B+M+I mice analyzed by Western blotting to detect NUAK2 and YAP1, which are normalized to GAPDH. (F) Pie charts demonstrating the distribution of HCC cases with $IQGAP1^{High}$ expression from the TCGA cohort. Distribution further breaks down the number of cases with $IQGAP1^{High}$ that also contain $NUAK2^{High}$ expression. (G) Overall survival for a subset of patients with $IQGAP1^{High}/NUAK2^{High}$ expression compared to $IQGAP1^{Unaltered}/NUAK2^{Unaltered}$ patients. (H) RNA-sequencing data from the TCGA samples with elevated *IQGAP1*/*NUAK2* expression compared to those without was used for IPA analysis to determine molecular pathways that are activated/inhibited (left) with corresponding changes to the genes that regulate respective molecular pathways (right). Graphs show means ± SEM, and dots represent individual mice. Data in panels A to C are representative of studies replicated in multiple HCC cell lines. (G) Log-rank (Mantel-Cox) test was used to determine significance for survival curve, and Student's *t* test was used for all others. *, $P < 0.05$; **, $P < 0.01$; ****, $P < 0.0001$.

protein expression in B+M+I than B+M livers at the 4-week time point, while YAP1 protein expression remains unchanged (Fig. 8E). Together, these data suggest that IQGAP1 overexpression enhances YAP1 activity and NUAK2 expression, which contributes to enhanced HCC growth in the B+M model.

We propose that IQGAP1 stabilizes YAP1 activity by promoting NUAK2 expression during early stages of HCC oncogenesis. To further understand the clinical implications of the IQGAP1-NUAK2 axis in HCCs, we identified 20 of 371 HCC patients in The Cancer Genome Atlas (TCGA) with high *IQGAP1* mRNA expression (Fig. 8F). Intriguingly, *NUAK2* was high in 35% of these patients. Patients with *IQGAP1*^{High}/*NUAK2*^{High} expression exhibited worse survival than other HCC patients, although the trend was not significant ($P = 0.107$), mostly likely due to low sample size (Fig. 8G). Furthermore, transcriptomic analysis revealed activation of multiple progrowth and prosurvival signaling pathways in *IQGAP1*^{High}/*NUAK2*^{High} patients compared to other HCC patients (Fig. 8H). Taken together, our data suggest that IQGAP1 overexpression in tumors exacerbates Hippo/YAP signaling via enhanced NUAK2 expression, which may be a druggable mechanism for a specific subset of HCC patients.

DISCUSSION

Our results show that the overexpression of IQGAP1, a scaffold protein, in the background of oncogenic β-catenin and MET signaling can promote HCC in the murine liver. Consistent with our finding, IQGAP1 is frequently induced and is associated with a worse prognosis in human HCC (6–9, 58). Similar to β-catenin, a known HCC tumor driver, gain or loss of IQGAP1 is insufficient to drive spontaneous hepatocellular carcinogenesis (17, 59) (Fig. 1D and E). While *Ctnnb1*$^{-/-}$ mice develop a robust HCC response driven by PDGFRα signaling with DEN administration (60), this is counter to *Iqgap1*$^{-/-}$ mice compared to control mice (Fig. 2). However, under the right conditions, IQGAP1 overexpression can exacerbate HCC, demonstrating its role as a tumor driver (Fig. 5).

We and others have shown that IQGAP1 overexpression can promote Wnt/β-catenin signaling *in vitro* (9, 16) (Fig. 1B). However, coexpression of activated β-catenin and IQGAP1 fail to synergize, increasing neither β-catenin reporter activity *in vitro* (Fig. 1C) nor HCC formation *in vivo* (Fig. 1D and E). It is possible that the β-catenin plus IQGAP1 condition does not promote HCC development, since IQGAP1 overexpression shifts excess β-catenin to the cell membrane (Fig. 6A to C) (61–63). These results suggest IQGAP1 overexpression acts as a tumor suppressor by translocating β-catenin to the cell membrane. Intriguingly, we do not find alterations in Wnt signaling when IQGAP1 is overexpressed or in *Iqgap1*$^{-/-}$ livers after DEN administration (data not shown), despite previous studies showing that IQGAP1 facilitates β-catenin's nuclear translocation and activity (9, 16, 64). Why β-catenin signaling does not change in the absence of IQGAP1 warrants future investigation. We did find that *in vitro* knockdown of *IQGAP1* increased MET expression and activation (Fig. 4). MET expression was also modestly induced in *Iqgap1*$^{-/-}$ liver tumors, suggesting that this increase is compensatory to the loss of IQGAP1 expression, or IQGAP1 may regulate turnover of the MET protein.

On the other hand, we demonstrate that increased expression of IQGAP1 is sufficient to increase tumor burden and exacerbates HCC development in the B+M model (Fig. 5). This enhanced tumor burden is not driven by increased MET or Wnt signaling (Fig. 6). Even though IQGAP1 overexpression can enhance β-catenin activity *in vitro* (Fig. 1B) and significantly increase cytosolic β-catenin protein *in vivo* (Fig. 6A), we find that β-catenin and IQGAP1 colocalize at the cell membrane in B+M+I livers (Fig. 6C). This implies that a higher level of IQGAP1 prevents β-catenin nuclear translocation and is in line with a well-known mechanism regulated by IQGAP1 that enhances E-cadherin–β-catenin complexes at the adherens junctions (61–63, 65).

HCC tumors are heterogenous and are not driven by a singular oncogenic pathway, and IQGAP1 is known to enhance multiple oncogenic pathways (25, 26, 66). We found

one such pathway in our model to be the Hippo/YAP signaling pathway. IQGAP1 is known to interact with and modulate YAP activity (43, 44). We found significantly elevated expression of *Birc5*, a target strongly linked to YAP activity (42), when IQGAP1 is overexpressed in the B+M model (Fig. 6D). In addition, we found IQGAP1 cooperates with mutant (S127A) YAP1 *in vitro* (Fig. 7 and 8). Overexpressing IQGAP1 in the B+M model also results in enhanced nuclear YAP1 as early as 2 weeks after HCC induction (Fig. 7D and E). While YAP1 targets not involved in neoplasia remained unchanged when comparing B+M to B+M+I samples (Fig. 7F), we found NUAK2 expression is consistently higher when IQGAP1 is overexpressed, resulting in exacerbated YAP1 activity (Fig. 8A to E). To evaluate the translational relevance of these findings, we mined the TCGA database. Thirty-five percent of patients with high *IQGAP1* expression also had high *NUAK2* levels (Fig. 8F); these patients exhibited increased proliferative signaling pathways and poor survival (Fig. 8G and H). Additionally, these patient samples have no activating *CTNNB1* mutations (data not shown), which indicates therapies targeting IQGAP1 and/or NUAK2 are more beneficial. The IQGAP1-YAP1-NUAK2 axis needs to be studied in a larger cohort of patients to better understand how this molecular signature affects patient outcomes. Globally, there were about 953,000 liver cancer cases in 2017 (67). Considering that 1.9% of patients in the TCGA cohort have increased IQGAP1 and NUAK2 expression, this equates to roughly 18,000 patients per year worldwide. This is likely an underestimate due to our use of TCGA mRNA expression data, since IQGAP1 protein is elevated in 60 to 80% of HCCs (6–9).

In summary, we show that IQGAP1 acts as an HCC tumor driver by enhancing YAP1 signaling. IQGAP1 can demonstrate multiple functions in HCC by potentially saturating excess β-catenin and, in turn, activating YAP1 signaling. Therefore, targeting domain-specific interactions of IQGAP1 may be a useful strategy to combat hepatic tumorigenesis.

MATERIALS AND METHODS

Animals. The Institutional Care and Use Committee approved all mouse experiments. *Iqgap1*$^{+/+}$, *Iqgap1*$^{+/-}$, and *Iqgap1*$^{-/-}$ mice maintained on a 129/SVJ background (129-*Iqgap1*^{tm1aber}/VsJ) were used for all diethylnitrosamine (DEN) experiments. These mice were generated in Andrew Bernards's laboratory (Massachusetts General Hospital, Boston, MA, USA) and were obtained from Valentina Schmidt (Stony Brook University, New York, USA). FVB/NJ mice were obtained from the Jackson Laboratory (Bar Harbor, ME). Animals were housed at the University of Illinois at Urbana-Champaign on conventional racks or the University of Pittsburgh in Optimice cages (AnimalCare Systems, Centennial, CO) with Sani-Chip coarse bedding (P. J. Murphy, Montville, NJ) at 24°C on a 12/12-h light/dark cycle with lights on starting at 5 a.m. central standard time, corresponding to Zeitgeber time (ZT) 0. Genotype was confirmed by PCR analysis of genomic DNA from tail clips. Mice were allowed *ad libitum* access to water and either Teklad F6 Rodent Diet (8664; Envigo) or standard mouse chow (Purina ISO Pro Rodent 3000; LabDiet, St. Louis, MO). Mice were provided huts and running wheels for enrichment. All animals were sacrificed between 9 a.m. and noon daily.

Mouse experiments. Male ($n = 77$) littermate *Iqgap1*$^{+/+}$, *Iqgap1*$^{+/-}$, and *Iqgap1*$^{-/-}$ mice were injected with 5 mg/kg of body weight DEN (N0258; Sigma-Aldrich) in sterile 1× phosphate-buffered saline (PBS) at 12 to 15 days of age via intraperitoneal injection (10 μl/g body weight). Mice were sacrificed at both 20 weeks and 50 weeks after administration to assess tumor burden.

Six- to 8-week-old male FVB/NJ mice were used for hydrodynamic tail vein injections. Mice were injected with 20 mg of pT3-EF5α-hMet-V5, pT3-EF5α-S45Y-β-catenin-Myc, or pT3-EF5α-IQGAP1-HA, a combination of EF5α-hMet-V5 and pT3-EF5α-S45Y-β-catenin-Myc, or a combination of EF5α-hMet-V5, pT3-EF5α-S45Y-β-catenin-Myc, and pT3-EF5α-IQGAP1-HA along with the Sleeping Beauty transposase (SB) (0.8 mg) in a ratio of 25:1. Injections were diluted to a total of 2 ml of normal saline (0.9% NaCl) and injected into the lateral tail vein in 5 to 7 s.

At the time of sacrifice, blood was collected by retroorbital bleeding, and serum was separated by centrifugation and immediately stored at −80°C in opaque tubes. Liver, gonadal white adipose tissue, spleen, and quadriceps tissues were collected, weighed, and flash-frozen for analysis. A piece of each liver/tumor and the lungs were fixed in 10% formalin for histological analysis.

Body weight and LW/BW. Livers from experimental animals were excised, washed in PBS, and weighed. The percentage of the weight occupied by the liver was determined by dividing the liver weight by the total body weight of the mouse.

Cell lines. Human HepG2, Hep3B, Snu-449, and Huh7 hepatoma cell lines were obtained from the American Type Cell Culture (ATCC). HepG2, Hep3B, and Huh7 were maintained in 10% fetal bovine serum (FBS) (Atlanta Biologicals) in Dulbecco's modified Eagle's medium. Snu-449 cells were maintained in 10% FBS in RPMI 1640. Cells were incubated at 37°C in a humidified 5% carbon dioxide atmosphere.

Constructs used. pEGFP-IQGAP1 was a gift from David Sacks (plasmid number 30112; Addgene). Using this construct, a hemagglutinin (HA) tag was added to IQGAP1 and cloned via Gateway PCR

(Invitrogen, Carlsbad, CA) into a pT3-EF5α vector. pT3-EF1aH Yap S127A was a gift from Xin Chen (plasmid number 86497; Addgene). 8×GTIIC-luciferase (YAP1 luciferase reporter) was a gift from Stefano Piccolo (plasmid number 34615; Addgene). Additional constructs used can be found in Table S1 in the supplemental material.

Luciferase assay. Cell lines were transfected simultaneously with 400 ng TOPFlash firefly luciferase reporter or 400 ng YAP1 luciferase reporter (plasmid number 34615; Addgene) and 100 ng renilla luciferase constructs alongside either siRNA or expression constructs listed in Table S1 using Lipofectamine 2000 (Life Technologies). Transfected cells were harvested after 72 h and processed with a Dual-Luciferase reporter assay kit (Promega). Luciferase activity was detected with an Infinite M200 PRO microplate reader (Tecan, Männedorf, Switzerland). Relative luciferase activities of transfected plasmids are represented as the activity of firefly luciferase activity normalized to renilla activity.

Histology. Liver samples were fixed in formalin for >24 h. They were then processed and embedded in paraffin wax. Four- or five-micrometer sections were cut. For immunohistochemistry, sections were deparaffinized using xylene and graded ethanol (100 to 95%) washes and incubated in citric acid-based antigen retrieval (Vector Labs, Burlingame, CA). Following antigen retrieval, liver sections were treated with 3% hydrogen peroxide to quench endogenous peroxidase and blocked with either 5% normal goat serum in 5% bovine serum albumin in Tris-buffered saline with Tween 20 (TBST) or avidin-biotin blocking solution (SP-2001; Vector Labs). Slides were incubated with primary antibody followed by biotinylated secondary antibody or horseradish peroxidase (HRP)-conjugated secondary antibody (concentrations indicated in Table S2). Avidin-conjugated peroxidase (ABC kit PK-6100; Vector Labs) with ImmPACT DAB peroxidase substrate (SK-4105; Vector Labs) or DAB HRP substrate kit (SK-4100; Vector Labs) was used to visualize stained tissues. Sections were counterstained with modified Harris hematoxylin (72711; Richard Allen) dehydrated with ethanol and xylene washes and mounted with Permount (Fisher).

Briefly, H&E staining was performed after deparaffinization. Slides were first stained with hematoxylin and rinsed with water, followed by dipping in 5% glacial acetic acid. Shandon's bluing reagent (ThermoScientific, Kalamazoo, MI) was used to retain hematoxylin counterstain. Slides were then dipped in eosin for 1 min and dehydrated with ethanol and xylene washes, followed by mounting with Permount.

Quantification of GS-positive clusters. After sections were stained for GS, pericentral and ectopic GS regions were identified. Ectopic GS clusters are defined as 1 or more cells located immediately adjacent. ImageJ (National Institutes of Health, Bethesda, MD) was used to measure the area of defined GS clusters.

RNA isolation, qRT-PCR, and PCR. Total RNA from fresh liver and tumor samples collected at sacrifice was extracted using TRIzol solution (Invitrogen) and subjected to quantitative reverse transcriptase PCR (qRT-PCR) to quantify the expression of protein-coding genes. $A_{260/280}$ and bleach RNA gel were used to assess RNA quality. RNA with an $A_{260/280}$ of >2.0 and a 28S/18S RNA ratio of approximately 2 was used for further analysis. Complementary DNA (cDNA) synthesis and qRT-PCR were performed either as previously described (68) or using Moloney-murine leukemia virus (Life Technologies), followed by qPCR performed with SYBR green PCR master mix (Life Technologies), Bullseye EvaGreen PCR master mix (Midwest Scientific), or TaqMan probes (Life Technologies) with TaqMan Universal master mix II (Life Technologies). Primer sequences and TaqMan probe identifiers (IDs) are described in Table S3. Reactions were performed using a StepOnePlus system (Life Technologies). Relative expression was calculated using the $\Delta\Delta C_T$ method. *Gapdh* was used as a housekeeping gene.

TaqMan probe IDs and primer sequences are listed below. Reactions were performed using a StepOnePlus system (Life Technologies).

DNA mutation analysis. Genomic DNA was isolated from DEN-induced liver tumors at 50 weeks posttreatment using QIAamp Fast DNA tissue kit (Qiagen). Fluidigm technology was used to sequence the DNA using four primer sets (Table S4). The read files were demultiplexed by primer and then by sample. Fastp, version 0.19.5, was used to perform quality filtering and trimming of the raw reads. The files were qc-trimmed and aligned to the mouse reference genome, version GRCm38.p6, with NCBI WebBlast to obtain the absolute coordinates in the forward strand version of the genome with bwa, version 0.7.17, using default parameters. Bam-read count, version 0.8, was run to generate the read counts at each of the locations identified. A customized R script then was run to generate a summary of nucleotide frequencies at the codons of interest. The base pair with the lowest percentage of reads matching the wild-type sequence was used to determine the prevalence of mutation at that codon in each sample.

Western blotting. Whole-tissue protein lysates were prepared from approximately 50 mg frozen tissue using SDS-based lysis buffer (50 mM Tris-HCl [pH 8.0], 10 mM EDTA, 1% SDS) containing protease/phosphatase inhibitors (radioimmunoprecipitation assay [RIPA] buffer). Lysates were removed to a fresh 1.5-ml tube and centrifuged at 18,400 × *g* for 10 min at 4°C to remove clear supernatant to a new 1.5-ml tube while disposing of the pellet. Samples were stored at −80°C until utilization or determination of protein concentration via bicinchoninic acid (BCA) protein assay (Fisher) to ensure equal protein concentrations for subsequent assays. For Western blotting, 50 to 200 μg total protein was loaded onto 8% to 12% SDS-PAGE gels. Proteins were transferred to Immobilon-P polyvinylidene difluoride membrane (IPVH00010; Millipore) either for 1 h at 100 V at 4°C or overnight at 35 V and 4°C. After transfer, the membranes were blocked in either 5% nonfat dry milk or 5% BSA dissolved in Blotto (0.15 M NaCl, 0.02 M Tris [pH 7.5], 0.1% Tween in distilled H_2O), followed by incubation with antibodies described in Table S2. Membranes were exposed to SuperSignal West Pico chemiluminescent substrate (Thermo Scientific Pierce, Pittsburgh, PA) for 1 to 2 min at room temperature, and bands reflective of target proteins were

viewed by a ChemiDoc imaging system (Bio-Rad). Bands were quantified with ImageJ (National Institutes of Health, Bethesda, MD).

Nuclear/cytoplasmic fractioning. Whole-liver samples were processed either by using the NE-PER nuclear and cytoplasmic extraction kit (Life Technologies) by following the manufacturer's recommendations or lysed using SDS-free subcellular fractionation buffer (20 mM HEPES, 10 mM KCl, 2 mM $MgCl_2$, 1 mM EDTA, 1 mM EGTA) containing protease/phosphatase inhibitors. Samples were manually agitated and incubated on ice for 30 min prior to centrifugation at 3,000 rpm for 5 min at 4°C. The supernatant containing the cytosolic fraction was moved to a fresh, 1.5-ml tube, while the pellet was washed 5× with subcellular fractionation buffer. After a final wash, the nuclear pellet was lysed using TBS with 0.1% SDS. Samples were stored at −80°C until use in protein quantification and Western blotting as previously described.

Immunoprecipitation. Whole-liver samples were lysed using immunoprecipitation lysis buffer (20 mM Tris base, 150 mM NaCl, 1 mM EDTA, 1 mM EGTA, 1% TritonX, pH 7.5) containing protease/phosphatase inhibitors. Samples were manually agitated and incubated on ice for 30 min prior to centrifugation at 15,000 rpm for 15 min at 4°C. Supernatants were removed to a fresh 1.5-ml tube, while the pellet was discarded. Samples were stored at −80°C until utilization or determination of protein concentration via BCA protein assay (Fisher) to ensure equal protein concentrations. Equal amounts of protein from respective groups were pooled and precleared on ice using normal control mouse IgG (Life Technologies) for 30 min, followed by incubating with A/G Plus-agarose beads (Santa Cruz) overnight at 4°C with gentle agitation. Samples were centrifuged for 5 min at 3,000 rpm, and supernatants were removed to a fresh 1.5-ml tube together with 5 μg of β-catenin monoclonal antibody (Table S2) overnight at 4°C with gentle agitation. A/G Plus-agarose beads were applied to each sample overnight at 4°C with gentle agitation. The supernatant was then removed from beads via centrifugation to a fresh 1.5-ml tube, and the pellet was washed four times with PBS containing protease/phosphatase inhibitor to prevent the disruption of delicate protein-protein interactions. Samples were then processed for Western blotting as previously described.

Cell proliferation assay. Cells transfected with respective constructs were incubated overnight. Cells were then serum starved for 6 h prior to a 30-min incubation with 5-ethynyl-2¨-deoxyuridine (EdU) to a final concentration of 10 μM. Cells were washed with 1× PBS and fixed using 4% paraformaldehyde for 15 min, followed by a subsequent wash using 1× PBS. Cells were then stained for EdU using a Click-iT Alexa-647 EdU flow cytometry assay kit (Life Technologies) by following the manufacturer's instructions.

Data analysis. RNA-sequencing gene expression data from the Hepatocellular Carcinoma TCGA Firehose Legacy data set were downloaded from the cbioportal (www.cbioportal.org) (69, 70). Patients were separated into two cohorts, those that have amplified *IQGAP1* and *NUAK2* mRNA expression fitting a cutoff z-score threshold of ±2 and those without. Gene expression data were analyzed through the use of IPA (Qiagen Inc.; https://www.qiagenbioinformatics.com/products/ingenuitypathway-analysis) using an experimental *P* value of >0.02 and a false discovery rate q value of >0.04 (71). Canonical pathway amplification/downregulation was determined using a −log(*P* value) of <2.3 and a z-score of <2.5 while thresholding at 0.05. Fisher's exact test was used to determine the significance of pathway alterations. Finally, pathways were filtered for relevance to liver biology and disease pathogenesis. For survival analysis, clinical data from the TCGA were analyzed to determine overall survival calculated from diagnosis date to the death date or date of last contact, taking censoring into consideration. Overall survival was then calculated for the patients using Kaplan-Meier methods.

Statistical analysis. Data are expressed as means ± standard errors of the means (SEM). All statistical analyses were performed using GraphPad Prism software, version 7. For contingency data, χ^2 test was used to compare 3 groups and Fisher's exact test was performed to assess differences between 2 groups. One-way analysis of variance (ANOVA) with Bonferroni posttest was performed to compare 3 groups, while two-way ANOVA with Tukey's posttest was used to assess differences between two paired tissues (liver and tumor) in three groups. Asterisks in figures indicate a statistically significant difference between groups. Significance is defined as a *P* value of <0.05. Outliers were determined by Grubbs' test and were removed from analysis along with any paired data.

Study approval. Animal studies were approved by the Institutional Animal Care and Use Committees at the University of Illinois at Urbana-Champaign and University of Pittsburgh. All animal studies were carried out as outlined in the *Guide for the Care and Use of Laboratory Animals* (72).

Data availability. The raw sequence data have been uploaded to NCBI BioProject (http://www.ncbi.nlm.nih.gov/bioproject/629000).

SUPPLEMENTAL MATERIAL

Supplemental material is available online only.

SUPPLEMENTAL FILE 1, PDF file, 0.1 MB.

ACKNOWLEDGMENTS

IPA, licensed through the Molecular Biology Information Service of the Health Sciences Library System, University of Pittsburgh, was used for data analysis. We thank Mark Band and Chris Wright for sequencing and Chris Fields and Gloria Rendon, HPCBio, Roy Carver Biotech Center at UIUC, for their help with DNA mutational analysis.

Writing, review, and/or revision of the manuscript: H.L.E., E.R.D., A.W.D., and S.A. Technical or material support (experimental design, execution, and data and statistical analysis): H.L.E., E.R.D., J.T., S.P.M., A.W.D., and S.A. Study supervision: A.W.D. and S.A.

We acknowledge the following financial support: S.A., R01 DK113080 and ACS132640-RSG; A.W.D., R01 DK103645; H.L.E., F30 CA206495; "Pittsburgh Liver Research Center Clinical Biospecimen Repository and Processing Core, P30DK120531."

We have no conflicts of interest to report.

REFERENCES

1. Llovet JM, Ricci S, Mazzaferro V, Hilgard P, Gane E, Blanc JF, de Oliveira AC, Santoro A, Raoul JL, Forner A, Schwartz M, Porta C, Zeuzem S, Bolondi L, Greten TF, Galle PR, Seitz JF, Borbath I, Haussinger D, Giannaris T, Shan M, Moscovici M, Voliotis D, Bruix J, SHARP Investigators Study Group. 2008. Sorafenib in advanced hepatocellular carcinoma. N Engl J Med 359:378–390. https://doi.org/10.1056/NEJMoa0708857.
2. Martini A, Ceranto E, Gatta A, Angeli P, Pontisso P. 2017. Occult liver disease burden: analysis from a large general practitioners' database. United Eur Gastroenterol J 5:982–986. https://doi.org/10.1177/2050640617696402.
3. Kudo M, Finn RS, Qin S, Han KH, Ikeda K, Piscaglia F, Baron A, Park JW, Han G, Jassem J, Blanc JF, Vogel A, Komov D, Evans TRJ, Lopez C, Dutcus C, Guo M, Saito K, Kraljevic S, Tamai T, Ren M, Cheng AL. 2018. Lenvatinib versus sorafenib in first-line treatment of patients with unresectable hepatocellular carcinoma: a randomised phase 3 non-inferiority trial. Lancet 391:1163–1173. https://doi.org/10.1016/S0140-6736(18)30207-1.
4. Buday L, Tompa P. 2010. Functional classification of scaffold proteins and related molecules. FEBS J 277:4348–4355. https://doi.org/10.1111/j.1742-4658.2010.07864.x.
5. White CD, Brown MD, Sacks DB. 2009. IQGAPs in cancer: a family of scaffold proteins underlying tumorigenesis. FEBS Lett 583:1817–1824. https://doi.org/10.1016/j.febslet.2009.05.007.
6. White CD, Khurana H, Gnatenko DV, Li Z, Odze RD, Sacks DB, Schmidt VA. 2010. IQGAP1 and IQGAP2 are reciprocally altered in hepatocellular carcinoma. BMC Gastroenterol 10:125. https://doi.org/10.1186/1471-230X-10-125.
7. Chen F, Zhu HH, Zhou LF, Wu SS, Wang J, Chen Z. 2010. IQGAP1 is overexpressed in hepatocellular carcinoma and promotes cell proliferation by Akt activation. Exp Mol Med 42:477–483. https://doi.org/10.3858/emm.2010.42.7.049.
8. Xia FD, Wang ZL, Chen HX, Huang Y, Li JD, Wang ZM, Li XY. 2014. Differential expression of IQGAP1/2 in hepatocellular carcinoma and its relationship with clinical outcomes. Asian Pac J Cancer Prev 15:4951–4956. https://doi.org/10.7314/APJCP.2014.15.12.4951.
9. Jin X, Liu Y, Liu J, Lu W, Liang Z, Zhang D, Liu G, Zhu H, Xu N, Liang S. 2015. The overexpression of IQGAP1 and beta-catenin is associated with tumor progression in hepatocellular carcinoma in vitro and in vivo. PLoS One 10:e0133770. https://doi.org/10.1371/journal.pone.0133770.
10. Jameson KL, Mazur PK, Zehnder AM, Zhang J, Zarnegar B, Sage J, Khavari PA. 2013. IQGAP1 scaffold-kinase interaction blockade selectively targets RAS-MAP kinase-driven tumors. Nat Med 19:626–630. https://doi.org/10.1038/nm.3165.
11. Liang Z, Yang Y, He Y, Yang P, Wang X, He G, Zhang P, Zhu H, Xu N, Zhao X, Liang S. 2017. SUMOylation of IQGAP1 promotes the development of colorectal cancer. Cancer Lett 411:90–99. https://doi.org/10.1016/j.canlet.2017.09.046.
12. Schmidt VA, Chiariello CS, Capilla E, Miller F, Bahou WF. 2008. Development of hepatocellular carcinoma in Iqgap2-deficient mice is IQGAP1 dependent. Mol Cell Biol 28:1489–1502. https://doi.org/10.1128/MCB.01090-07.
13. Liu C, Billadeau DD, Abdelhakim H, Leof E, Kaibuchi K, Bernabeu C, Bloom GS, Yang L, Boardman L, Shah VH, Kang N. 2013. IQGAP1 suppresses TbetaRII-mediated myofibroblastic activation and metastatic growth in liver. J Clin Investig 123:1138–1156. https://doi.org/10.1172/JCI63836.
14. Hensel J, Duex JE, Owens C, Dancik GM, Edwards MG, Frierson HF, Theodorescu D. 2015. Patient mutation directed shRNA screen uncovers novel bladder tumor growth suppressors. Mol Cancer Res 13:1306–1315. https://doi.org/10.1158/1541-7786.MCR-15-0130.
15. Bessede E, Molina S, Acuna-Amador L, Dubus P, Staedel C, Chambonnier L, Buissonniere A, Sifre E, Giese A, Benejat L, Rousseau B, Costet P, Sacks DB, Megraud F, Varon C. 2016. Deletion of IQGAP1 promotes Helicobacter pylori-induced gastric dysplasia in mice and acquisition of cancer stem cell properties in vitro. Oncotarget 7:80688–80699. https://doi.org/10.18632/oncotarget.12486.
16. Briggs MW, Li Z, Sacks DB. 2002. IQGAP1-mediated stimulation of transcriptional co-activation by beta-catenin is modulated by calmodulin. J Biol Chem 277:7453–7465. https://doi.org/10.1074/jbc.M104315200.
17. Tao J, Xu E, Zhao Y, Singh S, Li X, Couchy G, Chen X, Zucman-Rossi J, Chikina M, Monga SP. 2016. Modeling a human HCC subset in mice through co-expression of Met and point-mutant beta-catenin. Hepatology 64:1587–1605. https://doi.org/10.1002/hep.28601.
18. Liu F, Song Y, Liu D. 1999. Hydrodynamics-based transfection in animals by systemic administration of plasmid DNA. Gene Ther 6:1258–1266. https://doi.org/10.1038/sj.gt.3300947.
19. Bell JB, Podetz-Pedersen KM, Aronovich EL, Belur LR, McIvor RS, Hackett PB. 2007. Preferential delivery of the Sleeping Beauty transposon system to livers of mice by hydrodynamic injection. Nat Protoc 2:3153–3165. https://doi.org/10.1038/nprot.2007.471.
20. Monga SP. 2020. "Inside-out" or "outside-in": choosing the right model of hepatocellular cancer. Gene Expr 20:139–145. https://doi.org/10.3727/105221620X15913805462476.
21. Vesselinovitch SD, Mihailovich N. 1983. Kinetics of diethylnitrosamine hepatocarcinogenesis in the infant mouse. Cancer Res 43:4253–4259.
22. Zoheir KM, Abd-Rabou AA, Harisa GI, Ashour AE, Ahmad SF, Attia SM, Bakheet SA, Abdel-Hamied HE, Abd-Allah AR, Kumar A. 2015. Gene expression of IQGAPs and Ras families in an experimental mouse model for hepatocellular carcinoma: a mechanistic study of cancer progression. Int J Clin Exp Pathol 8:8821–8831.
23. Kunimoto K, Nojima H, Yamazaki Y, Yoshikawa T, Okanoue T, Tsukita S. 2009. Involvement of IQGAP3, a regulator of Ras/ERK-related cascade, in hepatocyte proliferation in mouse liver regeneration and development. J Cell Physiol 220:621–631. https://doi.org/10.1002/jcp.21798.
24. Shi Y, Qin N, Zhou Q, Chen Y, Huang S, Chen B, Shen G, Jia H. 2017. Role of IQGAP3 in metastasis and epithelial-mesenchymal transition in human hepatocellular carcinoma. J Transl Med 15:176. https://doi.org/10.1186/s12967-017-1275-8.
25. Boyault S, Rickman DS, de Reynies A, Balabaud C, Rebouissou S, Jeannot E, Herault A, Saric J, Belghiti J, Franco D, Bioulac-Sage P, Laurent-Puig P, Zucman-Rossi J. 2007. Transcriptome classification of HCC is related to gene alterations and to new therapeutic targets. Hepatology 45:42–52. https://doi.org/10.1002/hep.21467.
26. Calderaro J, Couchy G, Imbeaud S, Amaddeo G, Letouze E, Blanc JF, Laurent C, Hajji Y, Azoulay D, Bioulac-Sage P, Nault JC, Zucman-Rossi J. 2017. Histological subtypes of hepatocellular carcinoma are related to gene mutations and molecular tumour classification. J Hepatol 67:727–738. https://doi.org/10.1016/j.jhep.2017.05.014.
27. Buchmann A, Karcier Z, Schmid B, Strathmann J, Schwarz M. 2008. Differential selection for B-raf and Ha-ras mutated liver tumors in mice with high and low susceptibility to hepatocarcinogenesis. Mutat Res 638:66–74. https://doi.org/10.1016/j.mrfmmm.2007.08.015.
28. Aydinlik H, Nguyen TD, Moennikes O, Buchmann A, Schwarz M. 2001. Selective pressure during tumor promotion by phenobarbital leads to clonal outgrowth of beta-catenin-mutated mouse liver tumors. Oncogene 20:7812–7816. https://doi.org/10.1038/sj.onc.1204982.
29. Dong P, Ihira K, Xiong Y, Watari H, Hanley SJ, Yamada T, Hosaka M, Kudo M, Yue J, Sakuragi N. 2016. Reactivation of epigenetically silenced miR-124 reverses the epithelial-to-mesenchymal transition and inhibits invasion in endometrial cancer cells via the direct repression of IQGAP1 expression. Oncotarget 7:20260–20270. https://doi.org/10.18632/oncotarget.7754.
30. Ren JG, Li Z, Sacks DB. 2007. IQGAP1 modulates activation of B-Raf. Proc Natl Acad Sci U S A 104:10465–10469. https://doi.org/10.1073/pnas.0611308104.

31. Roy M, Li Z, Sacks DB. 2004. IQGAP1 binds ERK2 and modulates its activity. J Biol Chem 279:17329–17337. https://doi.org/10.1074/jbc.M308405200.
32. Roy M, Li Z, Sacks DB. 2005. IQGAP1 is a scaffold for mitogen-activated protein kinase signaling. Mol Cell Biol 25:7940–7952. https://doi.org/10.1128/MCB.25.18.7940-7952.2005.
33. Bozkaya G, Korhan P, Cokaklı M, Erdal E, Sağol O, Karademir S, Korch C, Atabey N. 2012. Cooperative interaction of MUC1 with the HGF/c-Met pathway during hepatocarcinogenesis. Mol Cancer 11:64. https://doi.org/10.1186/1476-4598-11-64.
34. Monga SP, Mars WM, Pediaditakis P, Bell A, Mule K, Bowen WC, Wang X, Zarnegar R, Michalopoulos GK. 2002. Hepatocyte growth factor induces Wnt-independent nuclear translocation of beta-catenin after Met-beta-catenin dissociation in hepatocytes. Cancer Res 62:2064–2071.
35. Zeng G, Apte U, Micsenyi A, Bell A, Monga SP. 2006. Tyrosine residues 654 and 670 in beta-catenin are crucial in regulation of Met-beta-catenin interactions. Exp Cell Res 312:3620–3630. https://doi.org/10.1016/j.yexcr.2006.08.003.
36. Giordano S, Columbano A. 2014. Met as a therapeutic target in HCC: facts and hopes. J Hepatol 60:442–452. https://doi.org/10.1016/j.jhep.2013.09.009.
37. Hedman AC, McNulty DE, Li Z, Gorisse L, Annan RS, Sacks DB. 2020. Tyrosine phosphorylation of the scaffold protein IQGAP1 in the MET pathway alters function. J Biol Chem 295:18105–18121. https://doi.org/10.1074/jbc.RA120.015891.
38. Lee SH, Song IH, Noh R, Kang HY, Kim SB, Ko SY, Lee ES, Kim SH, Lee BS, Kim AN, Chae HB, Kim HS, Lee TH, Kang YW, Lee JD, Lee HY. 2015. Clinical outcomes of patients with advanced hepatocellular carcinoma treated with sorafenib: a retrospective study of routine clinical practice in multi-institutions. BMC Cancer 15:236. https://doi.org/10.1186/s12885-015-1273-2.
39. Peng SY, Chen WJ, Lai PL, Jeng YM, Sheu JC, Hsu HC. 2004. High alpha-fetoprotein level correlates with high stage, early recurrence and poor prognosis of hepatocellular carcinoma: significance of hepatitis virus infection, age, p53 and beta-catenin mutations. Int J Cancer 112:44–50. https://doi.org/10.1002/ijc.20279.
40. Imamura H, Matsuyama Y, Tanaka E, Ohkubo T, Hasegawa K, Miyagawa S, Sugawara Y, Minagawa M, Takayama T, Kawasaki S, Makuuchi M. 2003. Risk factors contributing to early and late phase intrahepatic recurrence of hepatocellular carcinoma after hepatectomy. J Hepatol 38:200–207. https://doi.org/10.1016/s0168-8278(02)00360-4.
41. Cox AG, Hwang KL, Brown KK, Evason K, Beltz S, Tsomides A, O'Connor K, Galli GG, Yimlamai D, Chhangawala S, Yuan M, Lien EC, Wucherpfennig J, Nissim S, Minami A, Cohen DE, Camargo FD, Asara JM, Houvras Y, Stainier DYR, Goessling W. 2016. Yap reprograms glutamine metabolism to increase nucleotide biosynthesis and enable liver growth. Nat Cell Biol 18:886–896. https://doi.org/10.1038/ncb3389.
42. Dong J, Feldmann G, Huang J, Wu S, Zhang N, Comerford SA, Gayyed MF, Anders RA, Maitra A, Pan D. 2007. Elucidation of a universal size-control mechanism in Drosophila and mammals. Cell 130:1120–1133. https://doi.org/10.1016/j.cell.2007.07.019.
43. Sayedyahossein S, Li Z, Hedman AC, Morgan CJ, Sacks DB. 2016. IQGAP1 binds to Yes-associated protein (YAP) and modulates its transcriptional activity. J Biol Chem 291:19261–19273. https://doi.org/10.1074/jbc.M116.732529.
44. Anakk S, Bhosale M, Schmidt VA, Johnson RL, Finegold MJ, Moore DD. 2013. Bile acids activate YAP to promote liver carcinogenesis. Cell Rep 5:1060–1069. https://doi.org/10.1016/j.celrep.2013.10.030.
45. Perra A, Kowalik MA, Ghiso E, Ledda-Columbano GM, Di Tommaso L, Angioni MM, Raschioni C, Testore E, Roncalli M, Giordano S, Columbano A. 2014. YAP activation is an early event and a potential therapeutic target in liver cancer development. J Hepatol 61:1088–1096. https://doi.org/10.1016/j.jhep.2014.06.033.
46. Park YY, Sohn BH, Johnson RL, Kang MH, Kim SB, Shim JJ, Mangala LS, Kim JH, Yoo JE, Rodriguez-Aguayo C, Pradeep S, Hwang JE, Jang HJ, Lee HS, Rupaimoole R, Lopez-Berestein G, Jeong W, Park IS, Park YN, Sood AK, Mills GB, Lee JS. 2016. Yes-associated protein 1 and transcriptional coactivator with PDZ-binding motif activate the mammalian target of rapamycin complex 1 pathway by regulating amino acid transporters in hepatocellular carcinoma. Hepatology 63:159–172. https://doi.org/10.1002/hep.28223.
47. Xu MZ, Chan SW, Liu AM, Wong KF, Fan ST, Chen J, Poon RT, Zender L, Lowe SW, Hong W, Luk JM. 2011. AXL receptor kinase is a mediator of YAP-dependent oncogenic functions in hepatocellular carcinoma. Oncogene 30:1229–1240. https://doi.org/10.1038/onc.2010.504.
48. Ahn EY, Kim JS, Kim GJ, Park YN. 2013. RASSF1A-mediated regulation of AREG via the Hippo pathway in hepatocellular carcinoma. Mol Cancer Res 11:748–758. https://doi.org/10.1158/1541-7786.MCR-12-0665.
49. Zhang J, Ji JY, Yu M, Overholtzer M, Smolen GA, Wang R, Brugge JS, Dyson NJ, Haber DA. 2009. YAP-dependent induction of amphiregulin identifies a non-cell-autonomous component of the Hippo pathway. Nat Cell Biol 11:1444–1450. https://doi.org/10.1038/ncb1993.
50. Zhao B, Ye X, Yu J, Li L, Li W, Li S, Yu J, Lin JD, Wang CY, Chinnaiyan AM, Lai ZC, Guan KL. 2008. TEAD mediates YAP-dependent gene induction and growth control. Genes Dev 22:1962–1971. https://doi.org/10.1101/gad.1664408.
51. Camargo FD, Gokhale S, Johnnidis JB, Fu D, Bell GW, Jaenisch R, Brummelkamp TR. 2007. YAP1 increases organ size and expands undifferentiated progenitor cells. Curr Biol 17:2054–2060. https://doi.org/10.1016/j.cub.2007.10.039.
52. Min Q, Molina L, Li J, Adebayo Michael AO, Russell JO, Preziosi ME, Singh S, Poddar M, Matz-Soja M, Ranganathan S, Bell AW, Gebhardt R, Gaunitz F, Yu J, Tao J, Monga SP. 2019. beta-catenin and Yes-associated protein 1 cooperate in hepatoblastoma pathogenesis. Am J Pathol 189:1091–1104. https://doi.org/10.1016/j.ajpath.2019.02.002.
53. Zhang J, Liu P, Tao J, Wang P, Zhang Y, Song X, Che L, Sumazin P, Ribback S, Kiss A, Schaff Z, Cigliano A, Dombrowski F, Cossu C, Pascale RM, Calvisi DF, Monga SP, Chen X. 2019. TEA domain transcription factor 4 is the major mediator of Yes-associated protein oncogenic activity in mouse and human hepatoblastoma. Am J Pathol 189:1077–1090. https://doi.org/10.1016/j.ajpath.2019.01.016.
54. Tao J, Calvisi DF, Ranganathan S, Cigliano A, Zhou L, Singh S, Jiang L, Fan B, Terracciano L, Armeanu-Ebinger S, Ribback S, Dombrowski F, Evert M, Chen X, Monga SPS. 2014. Activation of beta-catenin and Yap1 in human hepatoblastoma and induction of hepatocarcinogenesis in mice. Gastroenterology 147:690–701. https://doi.org/10.1053/j.gastro.2014.05.004.
55. LaQuaglia MJ, Grijalva JL, Mueller KA, Perez-Atayde AR, Kim HB, Sadri-Vakili G, Vakili K. 2016. YAP subcellular localization and hippo pathway transcriptome analysis in pediatric hepatocellular carcinoma. Sci Rep 6:30238. https://doi.org/10.1038/srep30238.
56. Yuan WC, Pepe-Mooney B, Galli GG, Dill MT, Huang HT, Hao M, Wang Y, Liang H, Calogero RA, Camargo FD. 2018. NUAK2 is a critical YAP target in liver cancer. Nat Commun 9:4834. https://doi.org/10.1038/s41467-018-07394-5.
57. Gill MK, Christova T, Zhang YY, Gregorieff A, Zhang L, Narimatsu M, Song S, Xiong S, Couzens AL, Tong J, Krieger JR, Moran MF, Zlotta AR, van der Kwast TH, Gingras AC, Sicheri F, Wrana JL, Attisano L. 2018. A feed forward loop enforces YAP/TAZ signaling during tumorigenesis. Nat Commun 9:3510. https://doi.org/10.1038/s41467-018-05939-2.
58. Schmidt VA. 2012. Watch the GAP: emerging roles for IQ motif-containing GTPase-activating proteins IQGAPs in hepatocellular carcinoma. Int J Hepatol 2012:958673. https://doi.org/10.1155/2012/958673.
59. Tan X, Behari J, Cieply B, Michalopoulos GK, Monga SP. 2006. Conditional deletion of beta-catenin reveals its role in liver growth and regeneration. Gastroenterology 131:1561–1572. https://doi.org/10.1053/j.gastro.2006.08.042.
60. Zhang XF, Tan X, Zeng G, Misse A, Singh S, Kim Y, Klaunig JE, Monga SP. 2010. Conditional beta-catenin loss in mice promotes chemical hepatocarcinogenesis: role of oxidative stress and platelet-derived growth factor receptor alpha/phosphoinositide 3-kinase signaling. Hepatology 52:954–965. https://doi.org/10.1002/hep.23747.
61. Li Z, Kim SH, Higgins JM, Brenner MB, Sacks DB. 1999. IQGAP1 and calmodulin modulate E-cadherin function. J Biol Chem 274:37885–37892. https://doi.org/10.1074/jbc.274.53.37885.
62. Fukata M, Kuroda S, Nakagawa M, Kawajiri A, Itoh N, Shoji I, Matsuura Y, Yonehara S, Fujisawa H, Kikuchi A, Kaibuchi K. 1999. Cdc42 and Rac1 regulate the interaction of IQGAP1 with beta-catenin. J Biol Chem 274:26044–26050. https://doi.org/10.1074/jbc.274.37.26044.
63. Kuroda S, Fukata M, Nakagawa M, Fujii K, Nakamura T, Ookubo T, Izawa I, Nagase T, Nomura N, Tani H, Shoji I, Matsuura Y, Yonehara S, Kaibuchi K. 1998. Role of IQGAP1, a target of the small GTPases Cdc42 and Rac1, in regulation of E-cadherin-mediated cell-cell adhesion. Science 281:832–835. https://doi.org/10.1126/science.281.5378.832.
64. Wang Y, Wang A, Wang F, Wang M, Zhu M, Ma Y, Wu R. 2008. IQGAP1 activates Tcf signal independent of Rac1 and Cdc42 in injury and repair of bronchial epithelial cells. Exp Mol Pathol 85:122–128. https://doi.org/10.1016/j.yexmp.2008.06.001.
65. Monga SP. 2014. Role and regulation of beta-catenin signaling during physiological liver growth. Gene Expr 16:51–62. https://doi.org/10.3727/105221614X13919976902138.

66. Hedman AC, Smith JM, Sacks DB. 2015. The biology of IQGAP proteins: beyond the cytoskeleton. EMBO Rep 16:427–446. https://doi.org/10.15252/embr.201439834.

67. Fitzmaurice C, Abate D, Abbasi N, Abbastabar H, Abd-Allah F, Abdel-Rahman O, Abdelalim A, Abdoli A, Abdollahpour I, Abdulle ASM, Abebe ND, Abraha HN, Abu-Raddad LJ, Abualhasan A, Adedeji IA, Advani SM, Afarideh M, Afshari M, Aghaali M, Agius D, Agrawal S, Ahmadi A, Ahmadian E, Ahmadpour E, Ahmed MB, Akbari ME, Akinyemiju T, Al-Aly Z, AlAbdulKader AM, Alahdab F, Alam T, Alamene GM, Alemnew BTT, Alene KA, Alinia C, Alipour V, Aljunid SM, Bakeshei FA, Almadi MAH, Almasi-Hashiani A, Alsharif U, Alsowaidi S, Alvis-Guzman N, Amini E, Amini S, Amoako YA, Anbari Z, Anber NH, Andrei CL, Anjomshoa M, Global Burden of Disease Cancer Collaboration, et al. 2019. Global, regional, and national cancer incidence, mortality, years of life lost, years lived with disability, and disability-adjusted life-years for 29 cancer groups, 1990 to 2017: a systematic analysis for the Global Burden of Disease Study. JAMA Oncol 5:1749. https://doi.org/10.1001/jamaoncol.2019.2996.

68. Erickson HL, Anakk S. 2018. Identification of IQ motif-containing GTPase-activating protein 1 as a regulator of long-term ketosis. JCI Insight 3:e99866. https://doi.org/10.1172/jci.insight.99866.

69. Cerami E, Gao J, Dogrusoz U, Gross BE, Sumer SO, Aksoy BA, Jacobsen A, Byrne CJ, Heuer ML, Larsson E, Antipin Y, Reva B, Goldberg AP, Sander C, Schultz N. 2012. The cBio cancer genomics portal: an open platform for exploring multidimensional cancer genomics data. Cancer Discov 2:401–404. https://doi.org/10.1158/2159-8290.CD-12-0095.

70. Gao J, Aksoy BA, Dogrusoz U, Dresdner G, Gross B, Sumer SO, Sun Y, Jacobsen A, Sinha R, Larsson E, Cerami E, Sander C, Schultz N. 2013. Integrative analysis of complex cancer genomics and clinical profiles using the cBioPortal. Sci Signal 6:pl1. https://doi.org/10.1126/scisignal.2004088.

71. Kramer A, Green J, Pollard J, Jr, Tugendreich S. 2014. Causal analysis approaches in Ingenuity Pathway Analysis. Bioinformatics 30:523–530. https://doi.org/10.1093/bioinformatics/btt703.

72. National Research Council. 2011. Guide for the care and use of laboratory animals, 8th ed. National Academies Press, Washington, DC.